

Mechanisms of subsurface thermal structure and sea surface thermohaline variabilities in the southwestern tropical Pacific during 1975-85

by Thierry Delcroix¹ and Christian Hénin¹

ABSTRACT

Major features of the southwestern tropical Pacific (SWTP), defined between 160E-140W and 24S-10S, are brought to light through analysis of surface water samples (23000) and temperature/depth observations (8500), both collected by ship of opportunity programs during the 1979-85 period.

The mean vertical thermal structure (and its related parameters), mean sea surface temperature (SST) and salinity (SSS) are first portrayed, to further quantify the 1979-85 variability. It is demonstrated that the observed seasonal and interannual variabilities, the latter being associated with the strong 1982-83 El Niño Southern Oscillation (ENSO) event, are mostly governed by specific mechanisms involving varying wind field and rainfall regimes.

During the non-ENSO period (1979-81 + 1984-85), SST annual cycle and 0-100 m thermal structure changes are tied to the seasonal variations of the sun's position (minimum SST in August). At the mean South Pacific Convergence Zone (SPCZ) position, there is a marked seasonal SSS cycle, with minimum SSS in March. This minimum occurs two to three months after maximum precipitation whose variations suffice to explain SSS changes, assuming a 28 ± 7 m mixed layer depth. It suggests that the seasonal SSS cycle is mostly governed by the rainfall regime associated with the SPCZ migration and intensity. During a "normal" year, the seasonal SPCZ migration causes local alternation of cyclonic and anticyclonic wind stress curls, so that west of 175W and between 13S-17S, the thermocline depth seasonal variations are governed by local Ekman pumping.

During the ENSO period (1982-83), notable changes in the vertical temperature distribution were mostly perceivable within 10S-15S and below 100 m, in response to an anomalous wind stress field that strongly raises the thermocline through local Ekman pumping (as much as 70 m in May 1983). The resulting thermocline shoaling intensified the southern branch of the south equatorial current, and induced a southward shift of the subtropical gyre center, as already observed during the 1957 and 1972 ENSO. In addition, it modified the whole water column all the way to the surface, and was thus responsible for the SST cooling anomaly (-0.5°C to -1°C) observed in the northern SWTP (i.e. in the warm pool area). In the southern SWTP, similar SST cooling was concomitant with a positive latent heat flux anomaly ($>20\text{W} \cdot \text{m}^{-2}$) mostly resulting from an increase in the northward wind component. At the mean SPCZ position, the SSS augmented to as much as +1 in early 1983, mainly in response to a rainfall deficit resulting from the equatorward shift of the SPCZ, and also to unusual zonal salt advection and vertical mixing.

1. Groupe SURTROPAC, ORSTOM, B. P. A5, Nouméa, New Caledonia.

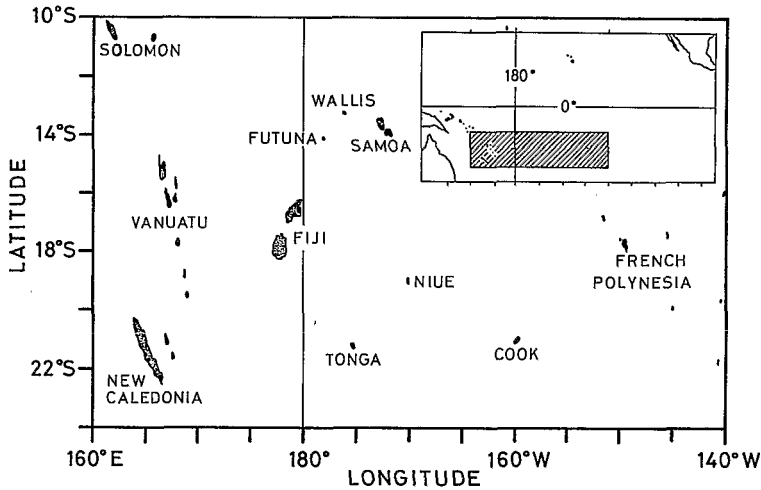


Figure 1. Location of the southwestern tropical Pacific in relation to the Pacific Ocean.

1. Introduction

Historical evidences of El Niño Southern Oscillation (ENSO) events first came from the south tropical Pacific. This was either from eye-witness reports of the Peru current reversal during the Conquistadores time (Quinn *et al.*, 1987), or four centuries later with Sir Walker's discovery of the SO (Walker, 1923). In recent years, meteorological observations have suggested that the origin of the SO must be sought in the South Pacific because well-arranged and strong anomalies were observed there long before anything comparable was seen in the northern hemisphere (Van Loon and Shea, 1985, 1987).

From an oceanographic point of view, the ENSO related modifications of the south tropical Pacific are rather poorly known due to the present disproportion between the amount of available data for the southern hemisphere and that for the northern hemisphere. Information on the south tropical Pacific Ocean has only been obtained in terms of climatological means (Donguy *et al.*, 1974; Reid and Arthur, 1975; Wyrski, 1975; Donguy and Hénin, 1978), or in the time domain along meridional sections from oceanographic cruises and/or Expandable Bathy-Thermograph (XBT) data (Rotschi *et al.*, 1972; Wyrski and Kilonsky, 1984; Kessler and Taft, 1987; Delcroix *et al.*, 1987). South of 10S, a basic description of the hydrological structure and an understanding of its variability are still lacking, especially with respect to the ENSO related impacts. The goal of this paper is to reduce this gap in our knowledge by focusing upon the Southwestern Tropical Pacific (SWTP) Ocean defined here between 24S–10S and 160E–140W (Fig. 1), during the 1979–85 period which includes the strong 1982–83 ENSO phenomenon.

This study directly concerns the population and States of the SWTP islands that

suffered ecologically and economically from the 1982–83 ENSO. It also concerns the air-sea interaction studies which are relevant to both the present TOGA (Tropical Ocean and Global Atmosphere) and future COARE (Coupled Ocean Atmosphere Response Experiment) programs (WCRP, 1985; Lukas and Webster, 1987). The SWTP is indeed an appropriate region to focus on in the frame of these programs. First, it is under the influence of the South Pacific Convergence Zone (SPCZ) which plays a key role in the development of wind, rainfall and convective activity variabilities (Kiladis and Van Loon, 1988; Von Storch *et al.*, 1988). Second, it partly belongs to the warm pool area (Sea surface temperature $>28^{\circ}\text{C}$) whose displacements may have a strong influence on midlatitude atmospheric circulation (Lukas, 1987). Third, it is situated between Tahiti, French Polynesia, and Darwin, Australia, where atmospheric sea level pressure records define the usual SO index (SOI). Finally, it should be noted that the SWTP presents the advantage of being particularly well monitored since 1979, through Ship of Opportunity Programs (SOPs).

As will be shown, in Section 2, the SOPs have now produced the surface and subsurface data sets required for a comprehensive oceanic sampling of the SWTP. Thanks to these data sets, a general description of the mean and 1979–85 variability of the main SWTP subsurface and surface structures will be given in Section 3. Section 4 will relate this variability to the responsible mechanisms, which are identified and tested with special emphasis on the 1982–83 ENSO period. Finally, a conclusion will be given in Section 5.

2. Data and methods

a. Temperature profiles. The spatial distribution of the temperature profiles used in this study is presented in Figure 2. These profiles consist of: (a) 53% of XBT collected from a SOP operated jointly by the ORSTOM Centres in Nouméa (New Caledonia) and Papeete (French Polynesia), and the Scripps Institution of Oceanography in La Jolla (California), (b) 43% of XBT obtained (courtesy J. Picaut) from different other sources (Commonwealth Scientific Industrial Research Organization, Etablissement Principal du Service Hydrographique et Océanographique de la Marine, Fleet Numerical Oceanographic Center, Japan Oceanographic Data Center, National Oceanographic Data Center, ORSTOM cruises), and (c) 4% of STD/CTD (Salinity-Conductivity Temperature Depth) and Nansen bottle measurements. On the whole, about 8500 temperature profiles have been gathered in the SWTP for the 1979–85 period.

The temperature profiles (hereafter referred to as XBT) are concentrated along six ship routes (Fig. 2), between Fiji, French Polynesia, Japan, Panama, New Caledonia, southern Tuamotu Islands, and U.S.A., covering most of the SWTP area. It should be noted that the region south of 22S and between 180–150W is poorly sampled, and the conclusions to be derived in this region should thus be viewed with some caution. The

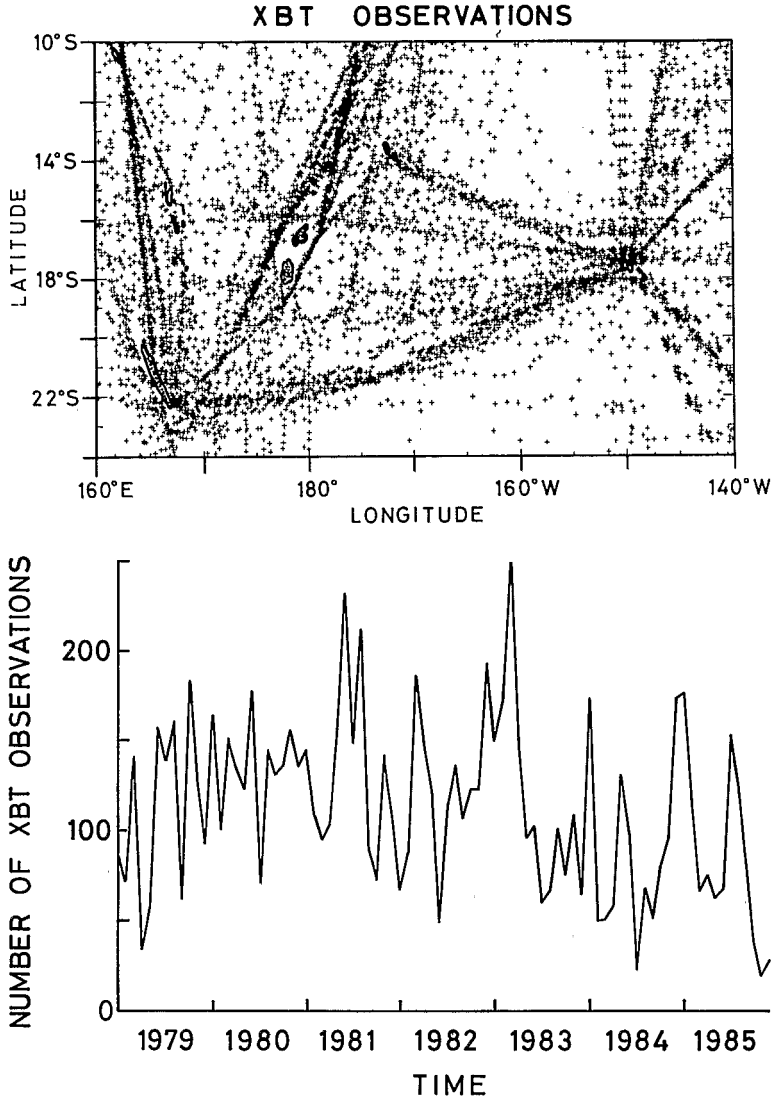


Figure 2. Spatial (top panel) and monthly (bottom panel) distributions of temperature/depth observations deployed during 1979–85 in the southwestern tropical Pacific.

XBT sampling rate (Fig. 2) is about $125 \text{ XBT} \cdot \text{month}^{-1}$ from the beginning of 1979 to early in 1983 with peaks in mid-1981 and at the end of 1982. It then decreases to the end of 1985 from 125 to about $75 \text{ XBT} \cdot \text{month}^{-1}$.

The XBT data validation was performed in a combination of both subjective and objective analyses, as reported in Delcroix and Hénin (1989). After quality control, the irregularly distributed space and time temperature data $T(x, y, z, t)$ were gridded in

longitude (x), latitude (y), depth (z) and time (t). The grid element size ($x = 10^\circ$, $y = 2^\circ$, $z = 5$ m and $t = 1$ month) was chosen to correspond to the space/time decorrelation scales of the region (White *et al.*, 1985), and it includes on a mean 2.7 temperature measurements. To construct a four-dimensional grid, the profiles were first grouped into seven 2.2° overlapping latitude bands centered on uneven integer latitudes from 23S to 11S. In each latitude band and for each depth, temperature data were then gridded using Laplacian interpolation. Finally, the seven latitude bands were merged to form the four-dimensional grid.

b. Surface samples. The entire set of surface samples (including bucket SST-SSS and atmospheric dry air temperature) was collected from a SOP operated jointly by the ORSTOM Centres in Nouméa (New Caledonia) and Papeete (French Polynesia), since 1969. The description of this data set is given here only for the bucket SSS measurements since it is quite representative of other surface samples.

The spatial distribution of the bucket SSS measurements is presented in Figure 3 for the 1979–85 period. The bucket SSS data set is composed of about 23000 observations, i.e. about thrice as much as the XBT observations shown in Figure 2 because commercial and French Navy ships were selected on regional routes between New Caledonia and different islands in addition to the ships equipped with an XBT system. The sampling rate (Fig. 3) is approximately $300 \text{ SSS} \cdot \text{month}^{-1}$ from January 1979 to November 1983 with peaks in late 1980–82 and early in 1983; it then decreases to the end of 1985 when it is about $240 \text{ SSS} \cdot \text{month}^{-1}$. The SSS samples were measured in Nouméa or Tahiti with an inductively coupled salinometer Autolab with a precision better than 0.01 (salinities in this paper will be given in SI units, not in parts per thousand).

Dubious SSS measurements were detected by objective criteria, as detailed in Delcroix and Hénin (1989). After the validation step, the irregularly distributed space and time salinity data $S(x, y, t)$ were gridded in longitude (x), latitude (y) and time (t) following the same grid size and procedures as for XBT gridding.

c. Empirical orthogonal function and mean value. To examine spatially and temporally linked variability of the oceanic parameters studied in the following sections, we chose to use Empirical Orthogonal Functions (EOF). This method has been described and used in many papers (e.g., Lorenz, 1956). In EOF analysis, a given parameter $P'(s, t)$, relative to its time averaged values $\langle P(s, t) \rangle$, is expressed as:

$$P'(s, t) = \sum_i [Ti(t) \cdot Si(s)] + \langle P(s, t) \rangle$$

where $Si(s)$ is the spatial distribution or eigenvector and $Ti(t)$ the associated temporal coefficient for mode i . This procedure provides a series of orthogonal eigenvectors, each of which contains a percentage of the temporal variability of the data, and thus makes

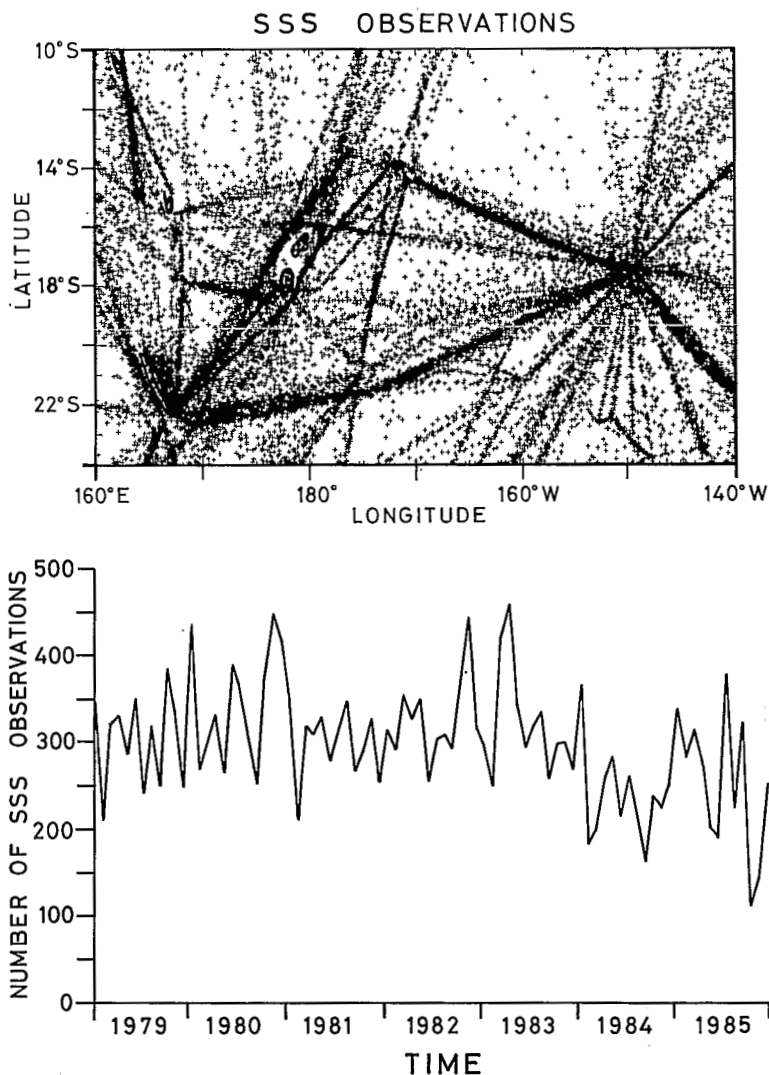


Figure 3. Spatial (top panel) and monthly (bottom panel) distributions of SSS observations deployed during 1979–85 in the southwestern tropical Pacific.

it possible to extract the main physical processes usually associated with the largest percentages.

The following sections will deal with the basic parameters of interest to ocean monitoring (SST, SSS, etc. . .). As a first step, each section will present mean and interannual Root Mean Square (RMS) maps to set the magnitude of each parameter prior to analyzing its space and time evolutions. Hence, the problem arose to define a mean situation within the 1979–85 period subject to the strong 1982–83 ENSO event

that, we thought, probably induced a non-Gaussian character in the SWTP subsurface thermal and surface thermohaline structures. Other researchers faced this problem in analyzing the short-term climatic variability of the Pacific Ocean during the 1979–82 period. Based on a local sea level study documenting a bimodal distribution (Meyers, 1982), White *et al.* (1985) and Pazan and White (1987) defined a mean situation over the three-year period 1979–81, while He and White (1987) for example included 1982 in their computation of the mean. To determine whether the 1982–83 period should be excluded from computation of the mean situation, in our particular SWTP region, monthly distributions of each parameter were plotted (not shown here) in different 2° latitude by 10° longitude boxes. Bimodal distributions mostly appeared in boxes situated north of about 16S for most parameters, with one mode being characteristic of the 1982–83 period. Hence, the mean situation will be defined over the five-year period 1979–81 + 1984–85 and the interannual RMS differences over the entire seven year period 1979–85.

3. The main structures

This section presents the main features of the SWTP, through an analysis of the basic subsurface and surface parameters (vertical thermal structure and the related heat content, dynamic height and geostrophic circulation, SST, and SSS), together with the wind field regime. The mean (1979–81 + 1984–85) structure and the 1979–85 variability are quantified for each parameter, in order to complement the description of the South Pacific Ocean, and to set the SWTP context, prior to focus, in the following section, upon the mechanisms that govern its variability.

a. Vertical thermal structure. Meridional temperature sections crossing the northern part of the SWTP may be found in the literature. From west to east are the section at 165E (Delcroix *et al.*, 1987; 20S–10N), the section at 170W (Kessler and Taft, 1987; 20S–10N), and the Hawaii to Tahiti Shuttle Experiment at 155W (Wyrtki and Kilonsky, 1984; 17S–20N). In a recent atlas, Delcroix and Hénin (1989) display annual and monthly means of meridional temperature sections along the 165E, 175W and 145W longitudes, from 24S to 10S. One important finding of these previous studies, as illustrated in our Figure 4, is the vertical spreading of the thermocline starting near 10S, as going southward, with a rise in the upper isotherms ($T > 20^{\circ}\text{C}$), a deepening of the lower ones, and quasi-horizontality of the 20°C isotherm. Schematically, the SWTP is in the transition zone between the vertical temperature distribution of the equatorial band and the one of the extra-tropical region.

Zonal temperature distribution (not shown here) evidences that the zonal temperature gradient changes sign south of about 15S/17S, where isotherms slope eastward in contrast with the westward isotherm slope observed along the equator (Lemasson and Piton, 1968).

The seasonal variations of the vertical thermal structure, deducible from the maps of

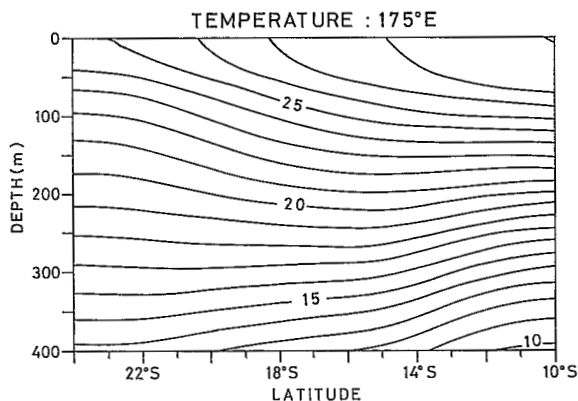


Figure 4. Latitude-depth diagrams of mean (1979–80 + 1984–85) isotherm depths at 175E.

Delcroix and Hénin (1989), are quantified here through a Fourier analysis over the 1979–81 + 1984–85 period. Figure 5 presents the amplitude of the annual harmonic of temperature along 175W as a function of latitude and depth, and along 19S as a function of longitude and depth. In a vertical plane, the annual harmonic amplitude of temperature is quite constant in the upper 25 m, then decreases sharply between

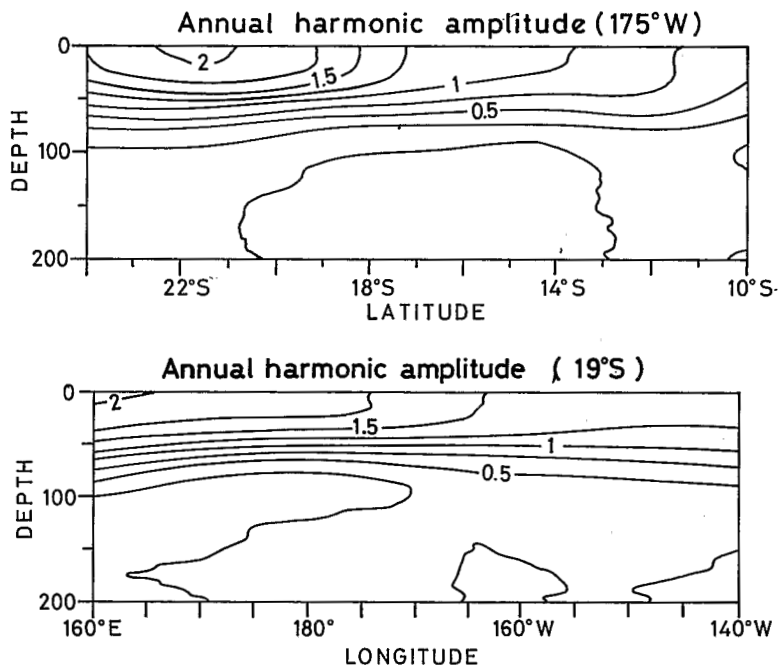


Figure 5. Top panel: latitude-depth diagrams of the annual harmonic amplitude of temperature at 175W longitude. Bottom panel: longitude-depth diagrams of the annual harmonic amplitude of temperature at 19S latitude. Contours are at 0.25°C intervals.

50 m and 100 m, and becomes negligible ($<0.25^{\circ}\text{C}$) below 100 m. In an horizontal plane, it increases both southward and westward in the upper 50 m.

b. Heat content (0–400 m). The 0–Zm Heat Content (HC) is defined here as the average temperature of the upper Zm. It is directly related to the usual HC definition through the product of density and heat capacity of sea water (C_p) and the Zm depth.

The mean 0–400 m HC and its interannual RMS are shown in Figure 6. South of 18S, the mean map shows zonal oriented iso-HC (19.4 to 20.4°C) with an almost regular meridional gradient. A relative maximum is then present in the 18S–14S band, and corresponds to the meridional slope reversal of warmer ($T > 20^{\circ}\text{C}$) isotherms (Delcroix and Hénin, 1989) which induces a geostrophic convergence. North of 14S, zonally oriented iso-HC (20.4 to 20.2°C) are observed east of 170W, and NE–SW oriented ones west of 170W with a minimum value reaching 19.6°C . This minimum, already observed and detailed in the literature (Oudot and Wauthy, 1976; Delcroix *et al.*, 1987), corresponds to isotherm doming probably associated with the divergence of the eastward flowing South Equatorial Counter Current (SECC) and the southern branch of the westward flowing South Equatorial Current (SEC).

The interannual RMS shows increased variability from 15S (0.4°C) to 10S (RMS $>0.7^{\circ}\text{C}$) mainly reflecting the ENSO signal. Indeed, the interannual RMS computed without the 1982–83 period (not shown here) is quite constant and ranges from 0.3 to 0.4°C in the whole SWTP. South of 15S, the interannual RMS is quite constant (0.4°C) with a slight increase south of 22S, west of the dateline.

The first EOF on 0–400 m HC is presented in Figure 7 and accounts for 43% of the total variance. The time function displays small variations, apart from the mid 1981–mid 1984 period during which the strong ENSO signal appears. The space function evidences that the ENSO phenomenon does not directly affect the latitudes south of about 15S, in agreement with the previous interannual RMS analysis. From our Figure 7, the ENSO signal may be decomposed into:

- (1) an accumulation of warm water from mid-1981 to March 1982,
- (2) a net release of heat between April 1982 and May 1983, with the onset occurring at the same time as in the north western equatorial Pacific (Delcroix and Gautier, 1987), and finally,
- (3) a return to “normal” situation only reached in 1984.

The first EOF on 0–400 m HC gives an insight into the redistribution of heat associated with the 1982–83 ENSO. However, it does not provide information on changes inside the 0–400 m layer since HC is an integrated quantity. To compare with the results of Section 3a, which demonstrated that it is mostly the upper 100 m layer that is affected by a seasonal variability, it is of interest to determine in which depth layer the interannual variability (i.e. the ENSO event) is most perceivable. To this end, we have focused our attention on the 10S–12S and 180–170W area which is the most

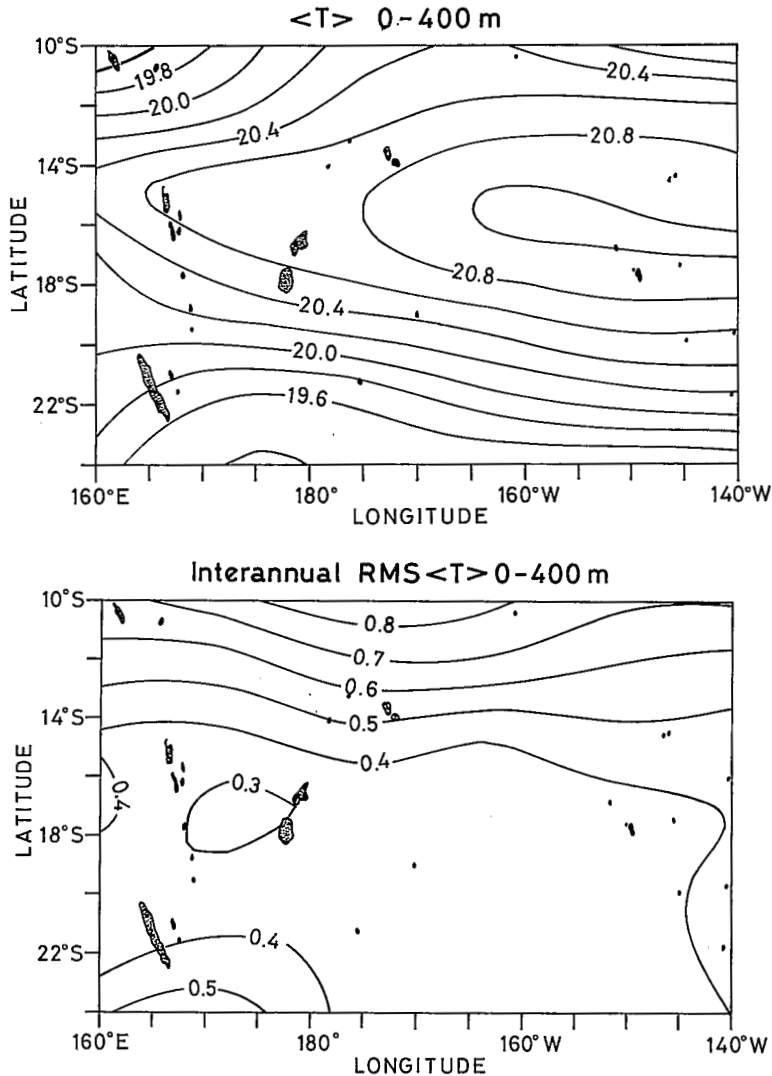


Figure 6. Top panel: mean (1979-81 + 1984-85) 0-400 m average temperature with contours at 0.2°C intervals. Bottom panel: interannual RMS (1979-85) with contours at 0.1°C intervals.

intensively XBT sampled region. This region is interesting because geographically it belongs to the warm water pool of the western Pacific Ocean. During the 1979-85 period, HC has been calculated for each month and for each of the four 0-100 m, 100-200 m, 200-300 m and 300-400 m layers. The low frequency variations of HC in the four layers are presented in Figure 8. In the upper 100 m, the ENSO signal is quite small compared with the 100-200 m and 200-300 m layers where peak to peak

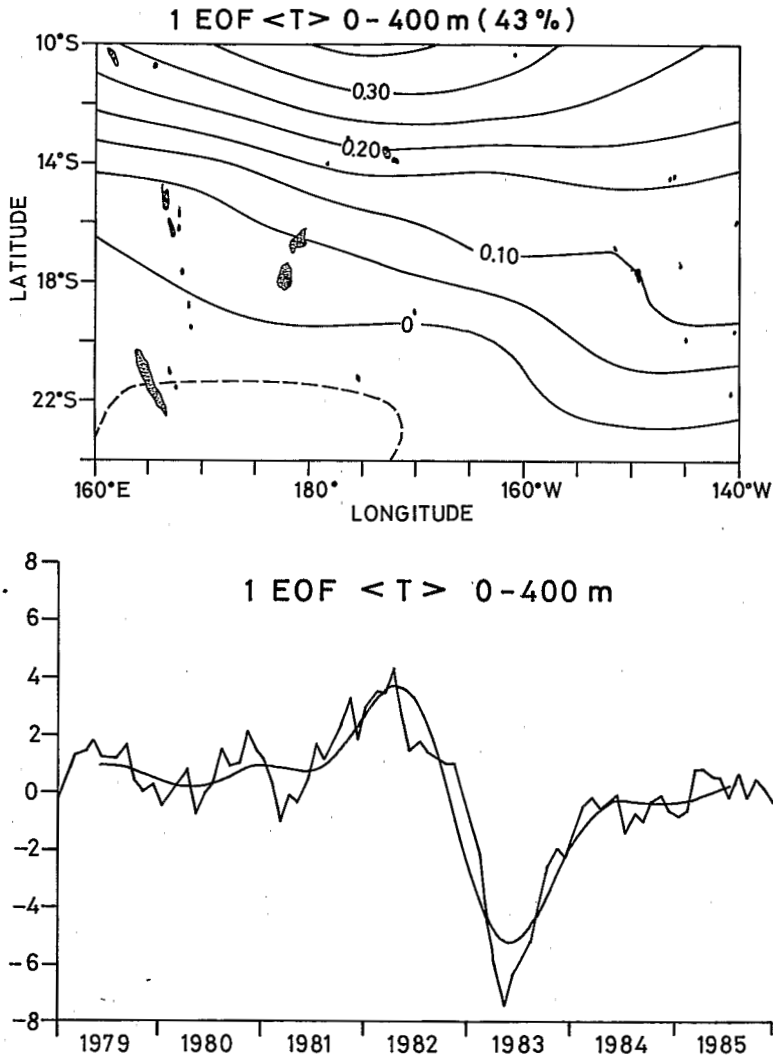


Figure 7. First empirical orthogonal function of the 0-400 m average temperature with spatial pattern (top panel) and time function (bottom panel). The broken line in the top panel denotes negative values. The low-frequency curve in the bottom panel is a result of a Fourier low pass filter removing period < 14 months.

variations reach more than 4°C . Hence, major changes related to the El Niño event occur between 100 m and 300 m, and not in the surface layer. In addition, it should be pointed out that accumulation of warm water occurs as early as the end of 1981, suggesting that ENSO forecasting efforts must take the SWTP into account.

The second EOF on HC 0-400 m (13% of the data variance) represents the annual cycle south of about 15°S , and is not shown here.

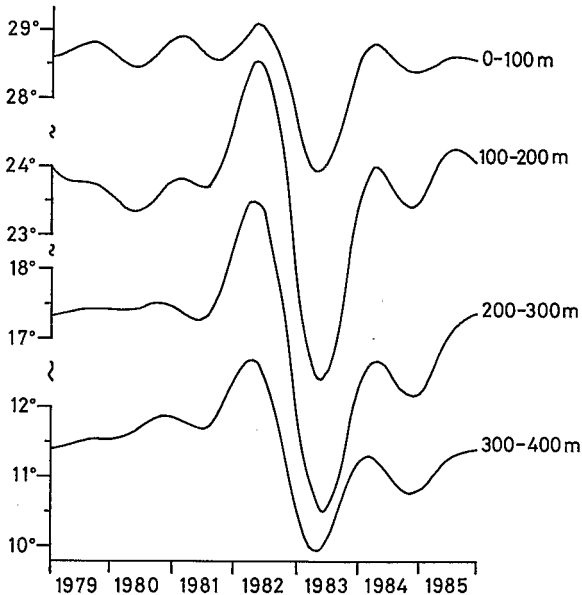


Figure 8. Low-frequency variations of the average temperature of the 0–100, 100–200, 200–300 and 300–400 m layers in the 10S–12S and 180–170W box.

c. Dynamic height and geostrophic circulation. Maps of mean surface dynamic height (re. 500 and 1000 db) over the SWTP may be derived from large scale dynamic height studies (Wyrтки, 1975-Fig. 1; Levitus, 1982-Fig. 56). Wyrтки's map shows that the northern boundary (10S) of the SWTP is situated half way between two ridges in dynamic height. One of these is centered at 8S, and the other ridge across the South Pacific from 13S–160E to 30S in the East Pacific. A shallow trough between these two ridges appears in Wyrтки (1975), but not in Levitus (1982). As discussed by Kessler and Taft (1987), the SECC lies between the northernmost of these ridges and the trough between, and the southern branch of the SEC, that lies between Wyrтки's southernmost ridge and the intervening trough. South of about 15S, both Wyrтки's and Levitus' maps show the northern part of the large scale anticyclonic gyre.

Thanks to our own temperature data set and to the mean Temperature-Salinity (TS) curves deduced from Levitus (1982), we computed dynamic height and zonal (U_g) and meridional (V_g) geostrophic current, through the well-known geostrophic equations. This procedure raises questions about (a) whether the mean TS curves used to deduce density profiles can reliably indicate fluctuations of geostrophic currents, and (b) whether the mean depth reached by the XBT (400 db) can be meaningfully used as a reference level. These questions have been addressed by numerous authors. Concerning the use of mean TS curves, Kessler and Taft (1987) and Delcroix *et al.* (1987) showed that the error in TS (comparing with true) dynamic height is of the order of 2 dyn·cm, with the maximum difference between TS and true dynamic height reaching

6 dyn·cm. Since zonal geostrophic current involves dynamic height gradient, it thus will be little altered when TS curve variations are quite uniform over the distance of derivation, i.e. 2° latitude in our case. Concerning the 400 db reference level, Delcroix *et al.* (1987) evidence a mean slope of roughly 1.2 dyn·cm·deg⁻¹ in dynamic height 400/1000 db in the western SWTP (165E), between 10 and 20S. This induces a U_g 0/400 db bias of +4 (11S) to +2 (19S) cm·s⁻¹, assuming that 1000 db is a level of no motion. On the other hand, Kessler and Taft (1987) conclude that 450 db is adequate for calculating dynamic height in the central SWTP (170W), while Wyrтки and Kilonsky (1984) argued that the reference level should be located below 500 m in the eastern SWTP (155W). From these contentions, deducing an error estimate for our geostrophic current is not easy, and we believe that values reported here should thus be considered as qualitative only, i.e. in error of ± 2 cm·s⁻¹.

The maps of dynamic height 0/400 db and U_g 0/400 db means are displayed in Figure 9. The quite large difference between Figure 9a and Figure 6a, the latter showing the map of heat content 0/400 m, emphasizes the importance of spatial salinity variations in the dynamic height. South of 15S, almost zonal oriented isodynamic heights 0/400 db (Fig. 9a) induce an eastward surface geostrophic current with maximum values (7 cm·s⁻¹) between 19S–21S in the vicinity of the dateline. This eastward flow denotes part of the large scale subtropical anticyclonic gyre (Merle *et al.*, 1969; Wyrтки, 1975; Levitus, 1982). North of 15S, the meridional dynamic height 0/400 db gradient changes sign and induces a westward surface U_g component which is the southern branch of the SEC (Wyrтки and Kilonsky, 1984; Kessler and Taft, 1987; Delcroix *et al.*, 1987). Surprisingly, we do not see the signature of the SECC at the northernmost end of Figure 9. It must mean that the average position of the related dynamic height trough, evidenced in Wyrтки (1975-Fig. 1), was north of 10S during 1979–81 + 1984–85, or that our 2° latitude gridding procedure smoothed the weak dynamic height relief between 11S and 13S. A zonal dynamic height gradient (0/400 db) also appears north of 15S, which induces an alternation of southward (west of 175W) to northward surface V_g component (not shown here). This V_g component (maximum 1 cm·s⁻¹) decreases poleward to the subtropical gyre center which extends, at the surface, from the Vanuatu Islands to French Polynesia (Wyrтки, 1975).

The mean latitude-depth diagram of U_g is presented in Figure 10 at longitude 175E. South of 15S, we observe the northern edge of the eastward flow representing part of the large scale anticyclonic gyre. At the surface, its northern boundary is situated around 15S in the whole SWTP region. It reaches 100/150 m depth, and its maximum velocity is situated at the sea surface and displaced southward from 16S–165E to 23S–145W (not shown here). North of 15S is part of the southern branch of the SEC with maximum velocity around 125 m, in agreement with profiling current meter spot measurement at 165E (Delcroix *et al.*, 1987). Current transports have been computed by integration over depth excluding all velocities less than 2 cm·s⁻¹ (integration without a cut-off leads to transport differing by a maximum of 12%). The mean eastward

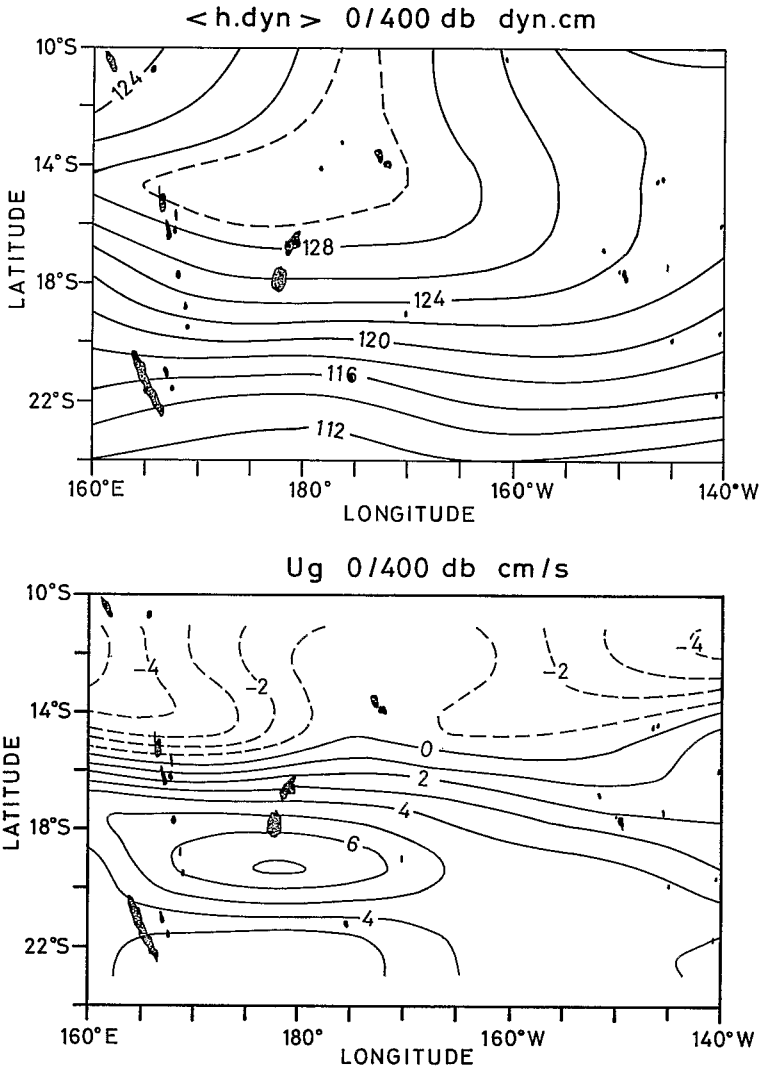


Figure 9. Top panel: mean (1979–81 + 1984–85) surface dynamic height (re. 400 db) with contours at 2 dyn · cm intervals, except for the broken line which denotes the 129 dyn · cm. Bottom panel: mean zonal surface geostrophic current U_g (re. 400 db) with contours at 1 cm · s⁻¹ intervals, negative values denote westward current. Note that the finite difference method used to compute U_g prohibits obtention of U_g values at 10S and 24S latitudes.

transport is $(3.7 \pm 1.7) \cdot 10^6 \text{ m}^3 \cdot \text{s}^{-1}$ (the second number is one standard deviation). It is quite small with respect to the equatorial current transports but only represents the northern side of a current which extends as far as the Antarctic Circumpolar Current. The mean westward transport is $(-6.3 \pm 2.5) \cdot 10^6 \text{ m}^3 \cdot \text{s}^{-1}$ but, once again, it must be noted that only part of its flow is sampled in the S WTP.

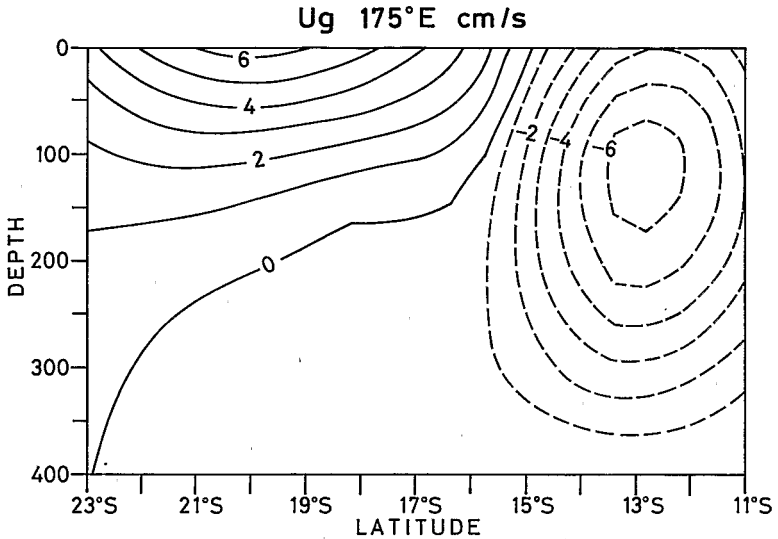


Figure 10. Latitude-depth diagram of the mean (1979–81 + 1984–85) zonal geostrophic current at 175E (re. 400 db) with contours at $1 \text{ cm} \cdot \text{s}^{-1}$ intervals. Negative values denote westward current.

The 1979–85 time series of eastward and westward geostrophic transports are displayed in Figure 11 for longitude 175E. The strongest variations occur during the 1982–83 ENSO when both transports are opposed in phase. As illustrated in Figure 12 during May 1983, these variations result from isotherm rises in the northern SWTP which both accentuate the meridional temperature gradient (i.e. the westward geostrophic velocity) and displace southward the center of the subtropical gyre (i.e. the surface occupied by the westward geostrophic velocity). Hence, the southern branch of

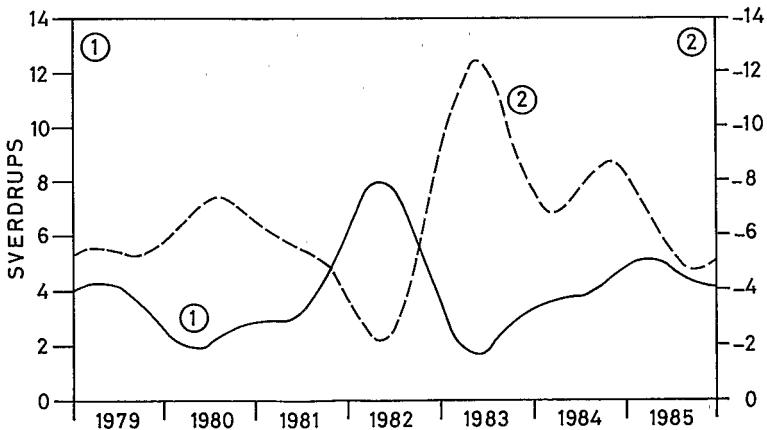


Figure 11. 1979–85 time series of eastward (1) and westward (2) geostrophic current transport (one Sverdrup is $10^6 \text{ m}^3 \cdot \text{s}^{-1}$) at 175E longitude, between 23S and 11S latitudes.

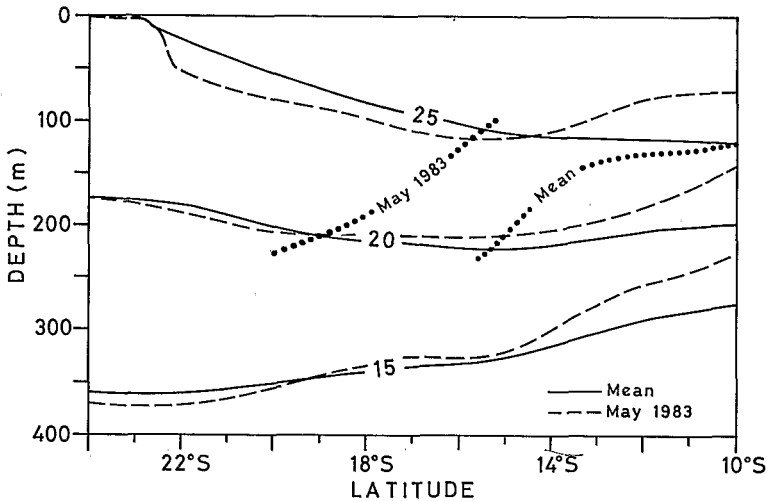


Figure 12. Latitude-depth diagram of the 15°C, 20°C and 25°C isotherm depths at 175E longitude, during the mean 1979–81 + 1984–85 (solid line) and May 1983 (broken line) periods. The dotted lines denote the subtropical gyre centers relative to the mean (10S–120 m to 16S–220 m) and May 1983 (16S–120 m to 20S–220 m) periods, as derived from the meridional slope reversal of each isotherm.

the SEC is most developed and overruns a large part of the SWTP, as was already observed in the western Pacific from the dateline to the Coral Sea (Donguy *et al.*, 1984; Donguy and Hénin, 1975) during the 1957 and 1972 El Niños. This confirms the poleward displacement of the anticyclonic gyre center in 1982–83, as already reported for the western SWTP from both sea level observations (Wyrtki, 1984) and XBT data (Meyers and Donguy, 1984).

d. Sea surface temperature. The values of SST could have been extracted either from the upper value of the XBT profiles, or from the bucket SST measurements. Estimation of the errors induced by the use of bucket measurements has already been amply documented, but comparisons between bucket and XBT-derived SST are rather sparse and somewhat inconclusive (Barnett, 1984; Folland *et al.*, 1984; Reverdin, 1988). The SST analysis was thus performed for each alternative (bucket and XBT) and the results were compared to each other in 2° latitude by 10° longitude data-rich areas of the SWTP, i.e. except south of 22S and between 180–150W where the poor XBT coverage prevented any reasonable estimate. On a mean, bucket SST is 0.1°C–0.2°C higher than XBT-derived SST, with a maximum difference of +0.3°C. This may stem from the fact that bucket measurement samples the surface value whereas XBT-derived SST is representative of the 3.5-meter depth. The precision of both bucket and XBT-derived SST was then estimated. Though bucket measurements are 2.7 times more numerous than XBT profiles, the standard deviations of the mean bucket SST

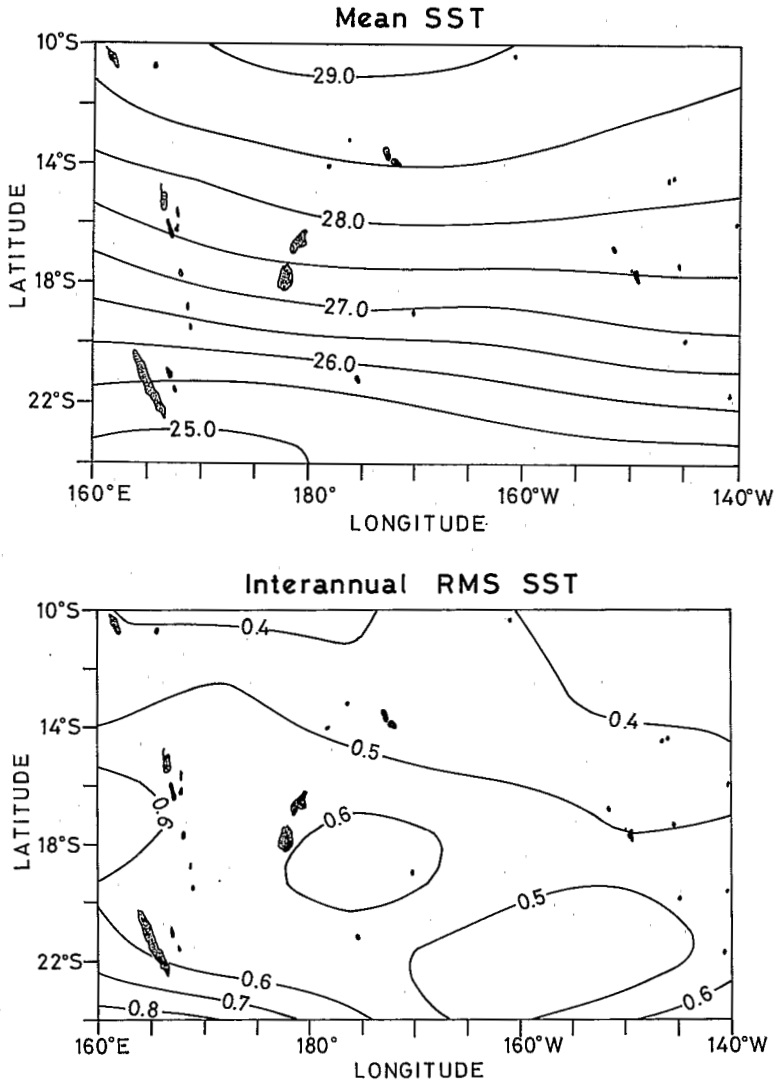


Figure 13. Top panel: mean sea surface temperature with contours at 0.5°C intervals. Bottom panel: interannual RMS of sea surface temperature with contours at 0.1°C intervals.

were about 25% greater than the ones computed from XBT-derived SST (mean value of 0.16°C versus 0.12°C). The results presented below thus used the upper value of the XBT profiles to represent SST. Note that values of SST thus only result from interpolation in the region sparsely covered by XBT (south of 22°S; 180–150°W), but bucket SST values available in this region evidence similar patterns for the figures discussed below.

The mean SST and its associated interannual RMS are presented in Figure 13. The

mean map shows almost zonally oriented isotherms with temperatures greater than 28°C north of 14S (i.e. in the warm pool) and less than 26°C south of 20S. This is in good agreement with Levitus (1982-Fig. 12), but about 0.5°C to 1°C less than values reported in White *et al.* (1985), even when averaging over the same 1979–81 period. This 0.5°C to 1°C difference is quite noteworthy with regard to the interannual RMS magnitude, but no convincing explanation has been found for the discrepancy which may be due to the fact that we used much more data. The seasonal variations of SST may be found in Delcroix and Hénin (1989). Interestingly, they show that the pool of warm water (SST >28°C) shifts northward (southward) during the austral winter (summer) to reach extremes of 12S (20S) latitude.

The interannual RMS of SST (Fig. 13) increases from the north (0.4°C) to the south (>0.6°C), and to a lesser extent, from the east (140W) to the west (160E). Its magnitude may denote phase shift or enhancement of the “normal” seasonal cycle as well as the 1982–83 ENSO event dissociated from this cycle. Exclusion of the 1982–83 period shows that the pattern of the interannual RMS (not shown here) is similar to that of Figure 13 with values lowered by 0.1°C. Hence, the interannual RMS magnitude mainly reflects modification of the normal seasonal cycle, its southward increase corresponding to a similar increase in the amplitude of the seasonal SST signal (e.g. 20% change in the amplitude of the “normal” seasonal cycle is 0.5°C at 24S and only 0.1°C at 10S). Still, it should be noted that the ratio of the interannual to annual RMS of SST ranges from 1 at 10S to 0.4 at 24S, illustrating the dominance of interannual SST signal in the northern versus the southern SWTP.

The first EOF on SST (Fig. 14) accounts for 82% of the data variance and primarily represents the seasonal cycle (minimum SST in August). The pattern of the eigenvector is very close to that of the annual harmonic amplitude because much of the variance is contained in the seasonal cycle. The annual harmonic amplitude, roughly given by the 1st EOF pattern multiplied by the amplitude of its associated time series, thus ranges from 0.5°C (10S) to a maximum of 2.5°C (24S). The interannual variability of SST is depicted by the low frequency curve in Figure 14. It evidences that SST:

- (1) was “normal” from 1979 to the end of 1981,
- (2) decreased from the beginning of 1982 to early 1983, and then
- (3) increased during 1.5 years to recover its “normal” values early in 1985.

This simplified scenario is close to the 1957–65–73–76 ENSO composite as given by Weare (1982), although our 1982–83 ENSO equivalent prior stage from June to November 1981 does not present warmer than usual SST (cf. Weare’s Fig. 1a). Similarly, it is in good agreement with the analysis of SST anomalies performed by Van Loon and Shea (1987), with still the exception of the equivalent June to November 1981 period. Since both analyses (Weare, 1982; Van Loon and Shea, 1987) did not include the period studied here, it is concluded that the change of SST anomalies was not “canonical” prior to the 1982–83 ENSO.

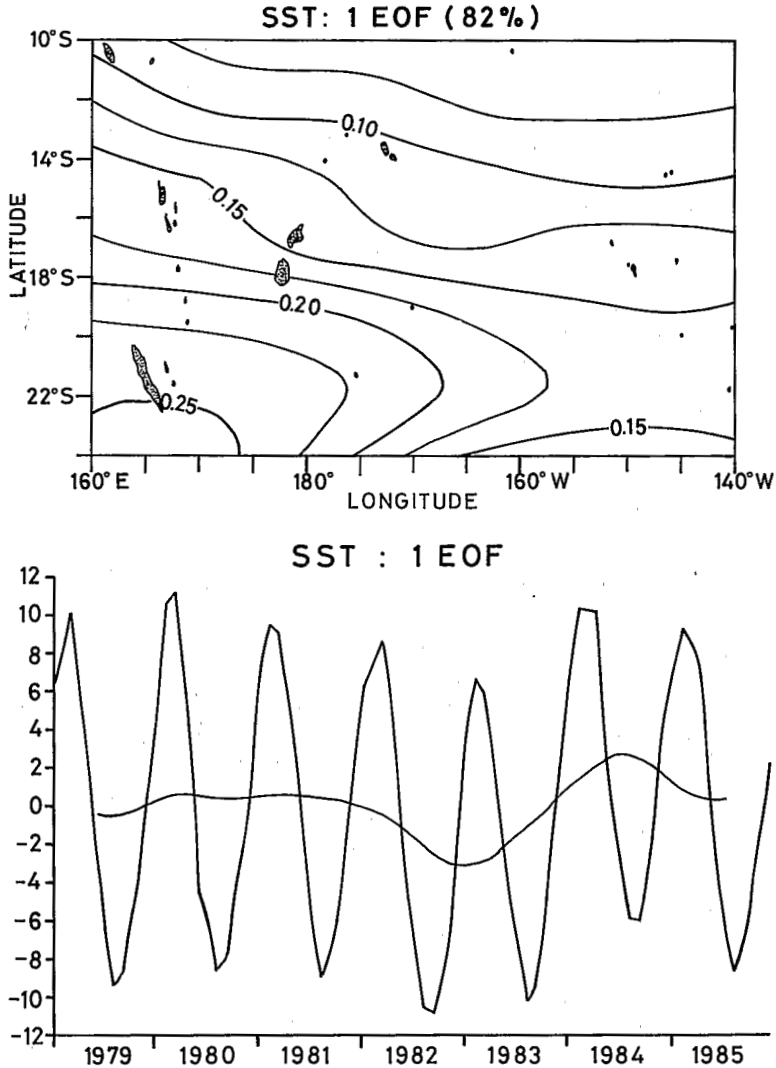


Figure 14. First empirical orthogonal function of the sea surface temperature with spatial pattern (top panel) and time function (bottom panel). The low-frequency curve in the bottom panel is a result of a Fourier low pass filter removing period < 14 months.

e. Sea surface salinity. The mean SSS and its associated interannual RMS are presented in Figure 15. The mean SSS distribution shows an almost SE/NW gradient between the high salinity waters ($S > 35.9$) of the central south tropical Pacific and the low ones ($S < 34.8$) north of the Vanuatu Islands where precipitation can reach $5 \text{ m} \cdot \text{year}^{-1}$ (Taylor, 1973). The SSS minimum coincides exactly with the evaporation minus precipitation ($E-P$) minimum (Donguy and Henin, 1976), indicating that advection and mixing would not play a major role in determining the SSS pattern.

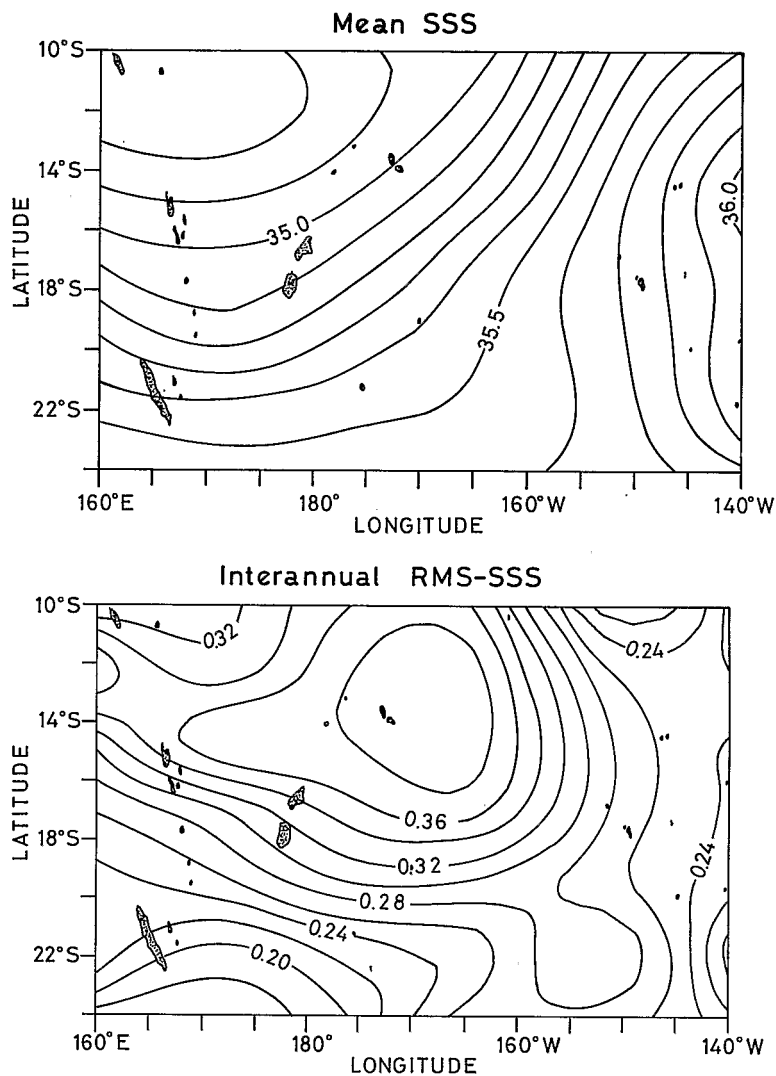


Figure 15. Top panel: mean sea surface salinity with contours at 0.1 intervals. Bottom panel: interannual RMS of sea surface salinity with contours at 0.02 intervals.

The interannual RMS map of SSS shows maximum values along a SE/NW axis characteristic of the mean SPCZ location that can be inferred either from mean precipitation, surface wind divergence or outgoing longwave radiation (Taylor, 1973; Pazan and Meyers, 1982; Heddinghaus and Krueger, 1981). A local RMS maximum (0.38) is situated where mean SSS gradient is the largest, suggesting important displacements of this salinity front. Inspection of monthly SSS maps (not shown here) and comparison with interannual RMS computed without the 1982–1983 period

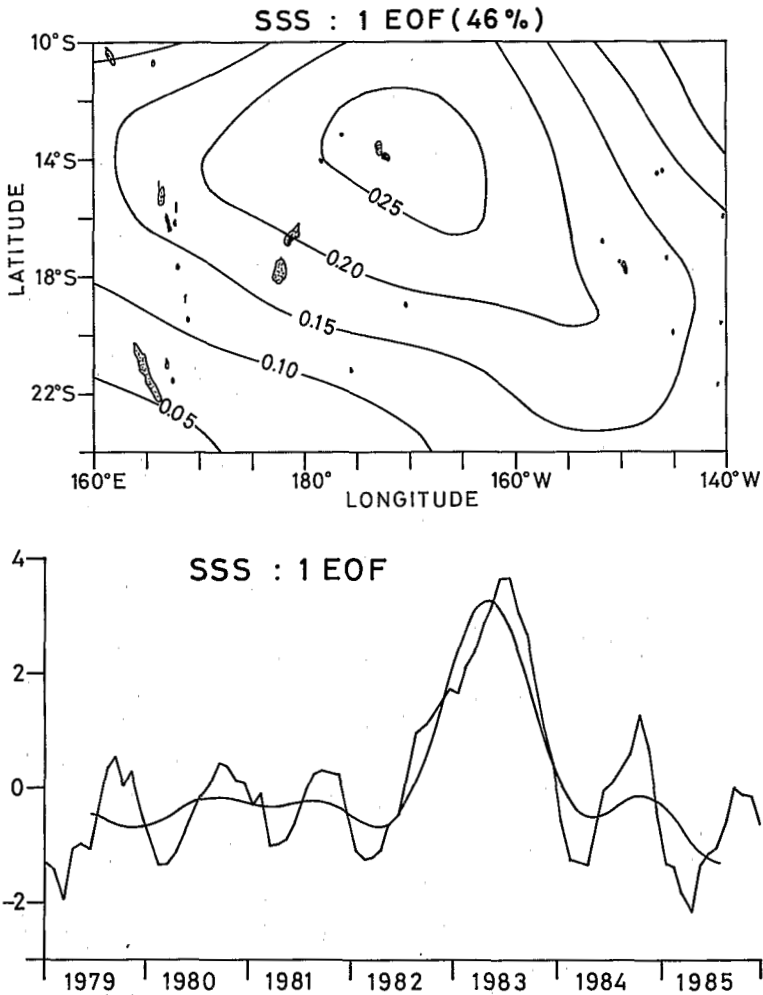


Figure 16. First empirical orthogonal function of the sea surface salinity with spatial pattern (top panel) and time function (bottom panel). The low-frequency curve in the bottom panel is a result of a Fourier low pass filter removing period <14 months.

confirms such displacements, and especially a N/NW migration of this front during the ENSO period.

The first EOF on SSS (Fig. 16) accounts for 46% of the data variance. The pattern of the eigenvector presents maximum values along the SPCZ axis. The time function together with the superimposed low frequency curve respectively depict the seasonal cycle during the 1979–81 + 1984–85 period (minimum SSS in March), and the interannual variability associated with the 1982–83 ENSO event. This emphasizes the strong ENSO signature upon SSS changes, its impact upon the SSS increase being thrice as much as the “usual” annual SSS cycle (+1 versus 0.2 along the mean SPCZ).

The second and third EOF extract only a total of 24% (13 + 11) and are not shown. A simple test of significance (North *et al.*, 1982) applied to the eigenvalues shows that these functions probably do not represent real physical phenomena.

f. Wind regime. The wind field analysis was performed from monthly mean pseudo-stress vectors (unit in $\text{m}^2 \cdot \text{s}^{-2}$) derived on 2° latitude by 2° longitude grids and obtained thanks to J. O'Brien of the Florida State University (FSU; cf. Goldenberg and O'Brien, 1981).

In the tropical Pacific Ocean, the northern and southern hemispheres are generally described as being mainly influenced by the NE and SE trade winds, respectively. However, it should be emphasized that the southern hemisphere presents two distinct systems of trade winds maintained by two high pressure cells located in the vicinity of Easter (109W; 29S) and Norfolk (168E; 29S) islands (cf. Rasmusson and Carpenter, 1982—Figs. 4–5). In this context, the FSU wind field shows (Fig. 17) that the SWTP is schematically concerned with: (a) SE (easterly) trade winds with maximum amplitude reaching about $6\text{--}7 \text{ m} \cdot \text{s}^{-1}$ north (south) of 17S during the austral winter (summer), (b) more zonally oriented trade winds in the east, especially in the austral summer, with mean amplitude of $5 \text{ m} \cdot \text{s}^{-1}$, and (c) the SPCZ spreading across the whole SWTP from north of Vanuatu toward French Polynesia. Note that the mean 1979–81 + 1984–85 FSU wind field is in good agreement with Wyrтки and Meyers (1976)'s analysis, with the notable exception that these authors show weak westerlies at about 12S in February (the extension of the NW Monsoon winds). The average annual cycle of the FSU wind divergence (not shown here) indicates that the SPCZ is less pronounced than the Inter Tropical Convergence Zone (ITCZ) and presents seasonal changes in both position and magnitude. In January, maximum convergence is observed near 15S in the SWTP when the associated convective activity brings maximum rainfall (Taylor, 1973), whereas in September the SPCZ is less marked and has shifted to the north, reaching about 10S.

In order to focus upon the interannual wind field variability, anomalies of the pseudo-stress components were computed with reference to the mean year (1979–81 + 1984–85), and contoured as a function of time and latitude, for each longitude. Examination of zonal anomalies (not shown here) did not reveal a close relationship between their magnitudes and the ENSO years. On the other hand, patterns of meridional anomalies are more interesting, as exemplified in Figure 18 which presents such anomalies averaged over 160E–140W. Two main periods of positive values, i.e. northward anomalies, are observed. The first period starts in mid-1979 and lasts for about one year when ENSO-like conditions were observed in the western Pacific although there was no basin-wide ENSO event (Donguy and Dessier, 1983). The second period, with the strongest positive anomalies, is centered in early 1983 and lasts for about eight months, i.e. concomitant with the strong 1982–83 ENSO. Over the SWTP, years with important northerly deviations thus correspond to ENSO-like or

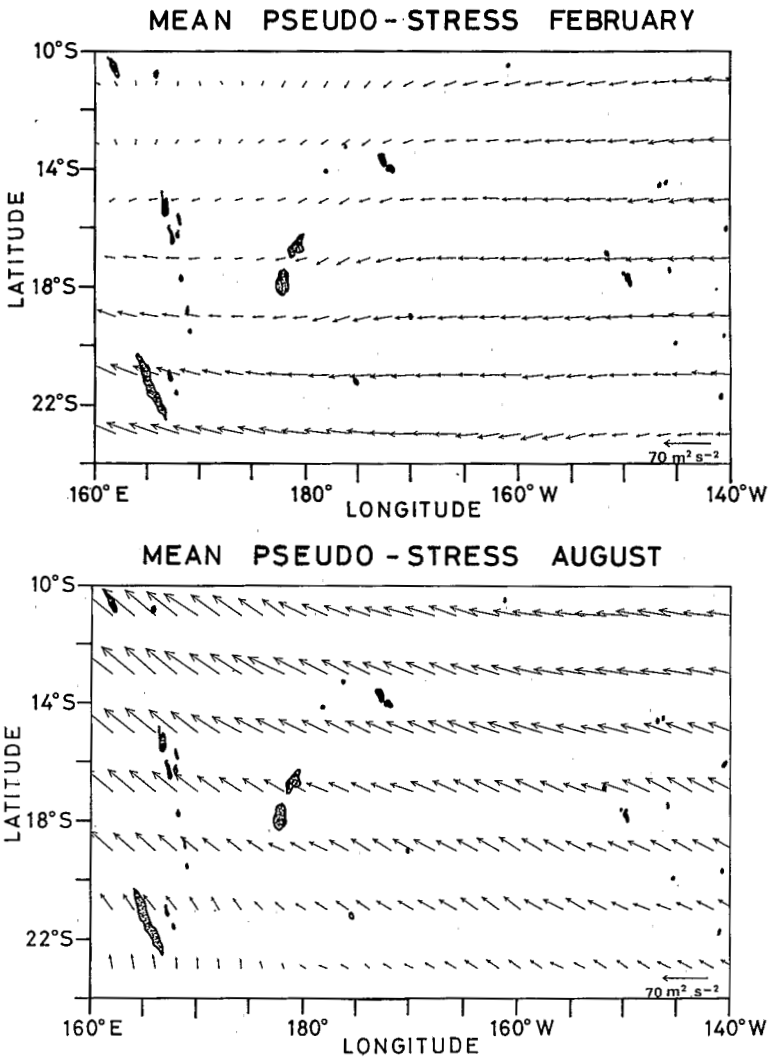


Figure 17. Mean (1979–81 + 1984–85) pseudo-stress ($\text{m}^2 \cdot \text{s}^{-2}$) in February (top panel) and August (bottom panel).

ENSO conditions, in agreement with similar conclusions obtained farther west during the 1965, 1973, 1976 and 1982 ENSO (Harrison, 1984; Mitchum, 1987).

4. Discussion on tentative explanatory mechanisms

After describing the main SWTP features, the purpose of this section is now to relate the observed 1979–85 subsurface and surface changes to specific mechanisms, with special emphasis upon the 1982–83 ENSO.

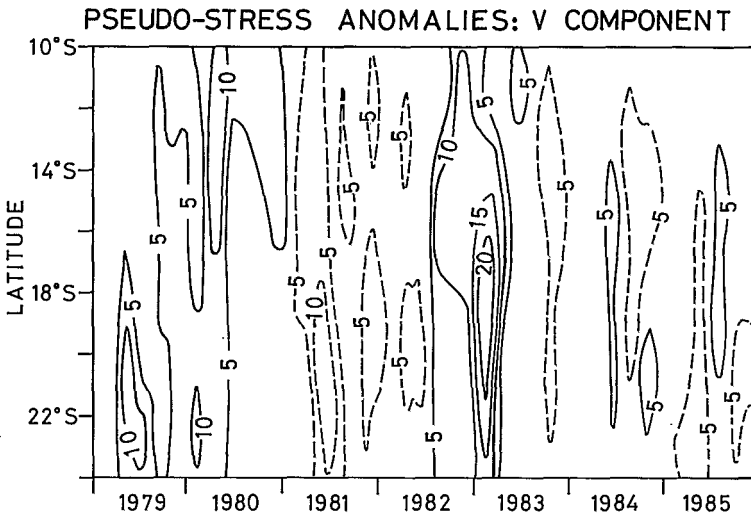


Figure 18. Anomalies of meridional pseudo-stress component averaged over 160E–140W. The reference is the 1979–81 + 1984–85 mean year. Contour intervals are $5 \text{ m}^2 \cdot \text{s}^2$ and solid (broken) lines denote southerly (northerly) anomalies.

a. Mechanisms of subsurface changes. In the extra equatorial SWTP region, the simplest dynamical mechanism that can modify the vertical thermal structure is Ekman pumping. The Ekman pumping mechanism states that divergence of the Ekman transport yields a vertical velocity at the bottom of the Ekman layer and thus vertically advects the thermocline in the absence of other active processes (Yoshida and Mao, 1957). The Ekman pumping dynamical balance is written as:

$$-\partial h / \partial t = \text{curl}_z (\tau / \rho \cdot f) \quad (1)$$

or

$$-\partial h / \partial t = \underbrace{[\text{curl}_z (\tau)]}_{(i)} + \underbrace{(\beta / f) \cdot \tau^x}_{(ii)} / \underbrace{(\rho \cdot f)}_{(iii)} \quad (2)$$

where h is the depth of the thermocline (>0 down), τ the wind stress vector (τ^x, τ^y) derived from pseudo-stress through Large and Pond (1981)'s formulae, ρ the density of sea water, f the Coriolis parameter and β its meridional (y) derivative. It is clear from Eq. 2 that the relative magnitude of the terms (II) and (III) will determine the sign of Ekman pumping. A qualitative description of these two terms is therefore presented first for a "normal" year (1979–81 + 1984–85), and for the 1982–83 ENSO period.

During a "normal" year, the zonal component of the wind stress is always negative (Fig. 17), i.e. eastward, so the term (III) is favorable to downwelling ($f < 0$) and adds a positive value to term (II). On the other hand, the term (II) can change sign in the course of the year as shown in Figure 19 for the mean February and August wind stress

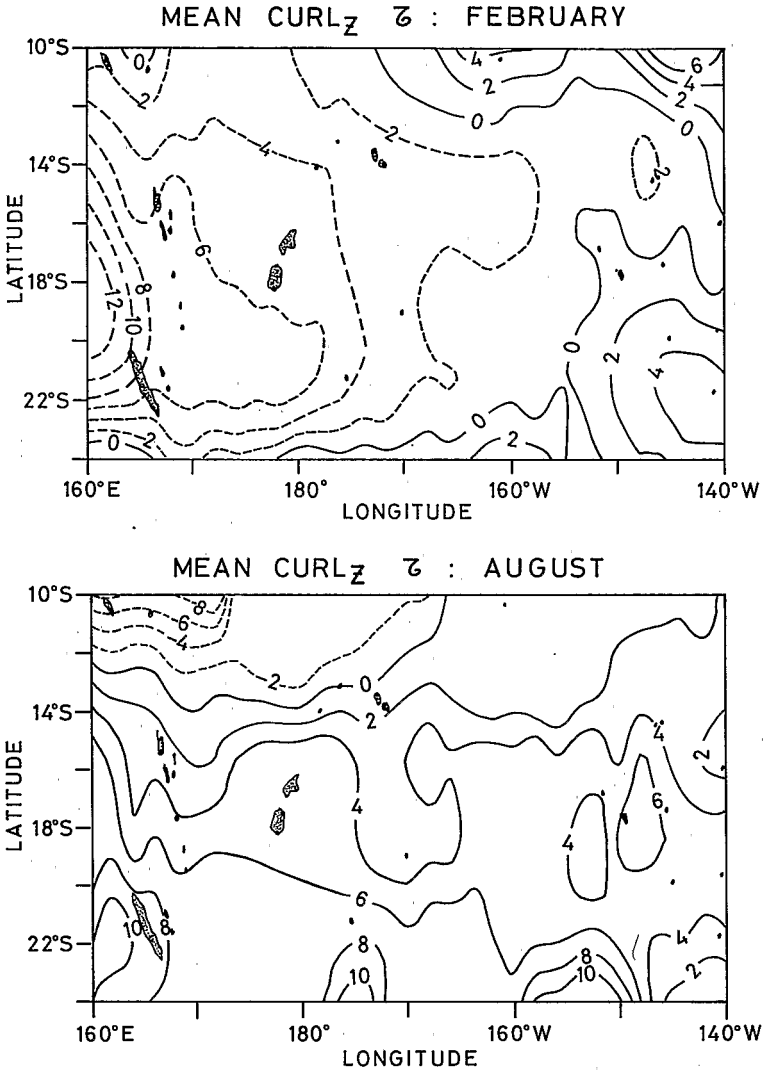


Figure 19. Mean (1979–81 + 1984–85) February and August wind stress curls. Contours are at $2 \cdot 10^{-8} \text{ N} \cdot \text{m}^{-3}$ intervals and the broken lines denote negative values.

curls. In February, the SPCZ overspreads the northern SWTP and induces a cyclonic (<0) curl west of 150°W . In August, when the SE trade winds are well developed, the SPCZ has shifted north of 10°S ; this produces, in contrast, an anticyclonic curl over most of the SWTP. Hence, the terms (II) and (III) add or balance, in such a way that the SWTP may be sliced into regions:

- (1) weakly affected by Ekman pumping (east of 170°W and south of 13°S ; west of 170°W and south of 19°S),

- (2) favorable to upwelling (west of 170W and north of 13S),
- (3) favorable to downwelling (east of 170W and north of 13S), and
- (4) propitious to the alternation of upwelling and downwelling depending on the period of the year (west of 170W and between 13S–19S).

During the 1982–83 ENSO period, drastic wind field changes were observed. Of main interest is the reversal of the zonal component of the wind stress ($\tau^x > 0$) in early 1983 between about 13S and the equator, as reported in atlases (e.g. Leetmaa and Witte, 1984), articles (e.g. Kessler and Taft, 1987) and deduced from the FSU wind field analysis (not shown here). At this time, the terms (II) and (III) act in the same way, leading to a strong positive (upward) Ekman pumping velocity in the northern SWTP.

Besides this qualitative approach, a quantitative comparison was performed between the two terms of Eq. 1, h being computed from the monthly values of the 20°C isotherm depth near 200 m. Because the corresponding time series were quite noisy, and since we are not interested in the month to month variability, they have been filtered in time to retain fluctuations in excess of five months (i.e. including the semiannual harmonic). Then, correlation coefficients R and R' between the two terms of Eq. 1 were derived, respectively, for the 1979–81 + 1984–85 (60-month length) and 1982–83 periods (24-month length). Note that there are roughly 60/5 and 24/5 degrees of freedom for R and R' , which indicates that 95% significance is obtained for correlation coefficients greater than 0.53 and 0.75. It is understood that the significance may be overestimated because of serial correlation between data points, but is believed to be statistically significant.

South of 18S, R and R' are less than 0.4 and the Ekman pumping balance does not hold. North of this latitude, time series of the two terms of Eq. 1 are presented for 15S and 11S latitudes (for 165E, 175W and 155W longitudes), to illustrate the comparisons (Fig. 20).

Latitude 15S: During the 1979–81 + 1984–85 period, fair agreement only exists west of 175W ($R = 0.71$), while the Ekman pumping balance does not hold ($R = 0.29$) in the eastern SWTP because the terms (II) and (III) almost cancel out. During 1982–83, good agreement ($R' > 0.7$) is observed between the two terms of Eq. 1 because the anomalous wind field patterns induce seasonal alternance of positive and negative $\text{curl}_z \tau$ whose amplitudes dominate $(\beta/f) \cdot \tau^x$ whatever the longitudes; when $\text{curl}_z \tau$ is < 0 in August 1982 and 1983, $(\beta/f) \cdot \tau^x$ only reinforces the Ekman pumping term. At 15S latitude, the thermocline depth variations are thus consistent with the preceding qualitative discussion.

Latitude 11S: During the 1979–81 + 1984–85 period the Ekman pumping velocity does not undergo seasonal changes and coefficient correlations R are thus quite low ($R < 0.35$). Indeed, as discussed in the qualitative approach, the terms (II) and (III)

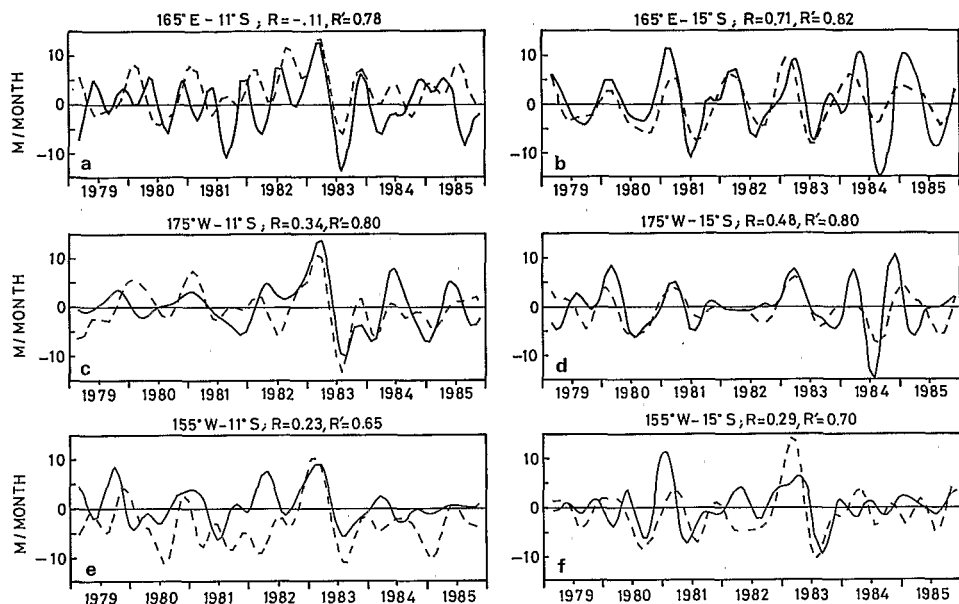


Figure 20. 1979–85 time series of the two terms of the Ekman pumping balance (see Eq. 1), at different reported locations. Solid line is $-\partial h/\partial t$, broken line is $\text{curl}_z(\tau/\rho \cdot f)$ in $\text{m} \cdot \text{month}^{-1}$ (the upward motion is positive). R and R' are, respectively, the correlation coefficients between the two terms during the 1979–81 + 1984–85 and 1982–83 periods.

lead to always positive Ekman pumping in the western SWTP (dashed line above 0 in Fig. 20a), and negative one in the eastern SWTP (dashed line below 0 in Fig. 20e) due to their relative magnitude. During the 1982–83 period the most pronounced thermocline depth and Ekman pumping variations are found. The anomalous wind field pattern ($\tau^x > 0$) observed in early 1983 raised the thermocline to as much as 70 m in May 1983 (Figs. 20a–c–e) since, as already noticed, the terms (II) and (III) act in the same way. Remarkably, local Ekman pumping is thus the main mechanism responsible for the very “unusual” 1982–83 upward isotherm movements in the northern SWTP ($R' > 0.7$), as well as for the related heat content and zonal geostrophic transport changes described in the preceding section.

During a “typical” year, our results somewhat contradict Kessler and Taft’s (1987) finding that Ekman pumping causes notable thermocline depth variations in the northern SWTP. This disagreement is probably caused by Kessler and Taft (1987)’s use of a different wind data set (i.e. Sadler and Kilonsky, 1985) which gives a more southern position of the mean SPCZ and wind curl patterns than the FSU wind used in this paper (see McPhaden *et al.*, 1988). However, we confirm and expand (in longitude) their results with regard to the role of the Ekman pumping mechanism during the 1982–83 ENSO.

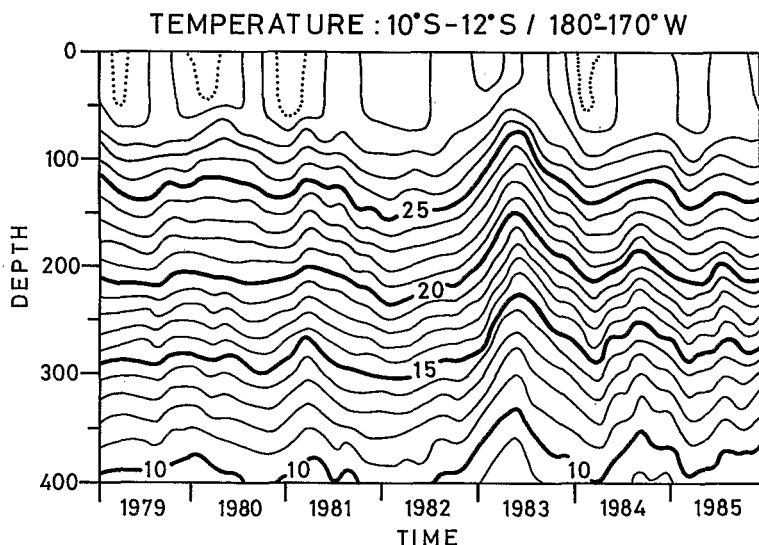


Figure 21. 1979-85 time series of isotherm depth in the (10S-12S; 180-170W) box. Contours are at 1°C intervals, except for the dotted line which is the 29.5°C isotherm.

b. Mechanism of sea surface temperature changes. The seasonal SST variations (Fig. 14) are very probably due to the net surface heat flux associated with the seasonal variations of the sun position (Stevenson and Niiler, 1983). Much more intriguing are the interannual SST variations, i.e. the negative anomalies observed in early 1983 (Fig. 14; low frequency curve). Relevant to the present TOGA and future COARE objectives, tentative explanations for these interannual variations are proposed here.

In the northern SWTP (10S-15S), the Ekman pumping mechanism may be responsible for the 1982-83 SST cooling anomaly because, as detailed in the previous section, it strongly raises the thermocline. So, the early 1983 SST cooling anomaly also reflects the underlying thermal structure changes. This is illustrated in Figure 21 which shows the 1979-85 time series of isotherm depth in the (10S-12S; 180-170W) box (corresponding to Fig. 8). There, it appears that Ekman pumping modifies the whole water column all the way to the surface, and clearly disturbs both the normal seasonal cycle and the usually quite constant SST.

In the southern SWTP (15S-24S), the latent heat flux variations may contribute to generating the discussed SST anomalies. The latent heat fluxes Q_e have been estimated from:

$$Q_e = \rho_a \cdot C_e \cdot L \cdot V \cdot (q_s - q_a) \quad (3)$$

or

$$Q_e = \rho_a \cdot C_e \cdot L \cdot V \cdot [e_s(T_s) - \gamma \cdot e_s(T_a)] \cdot (0.622/P_a) \quad (4)$$

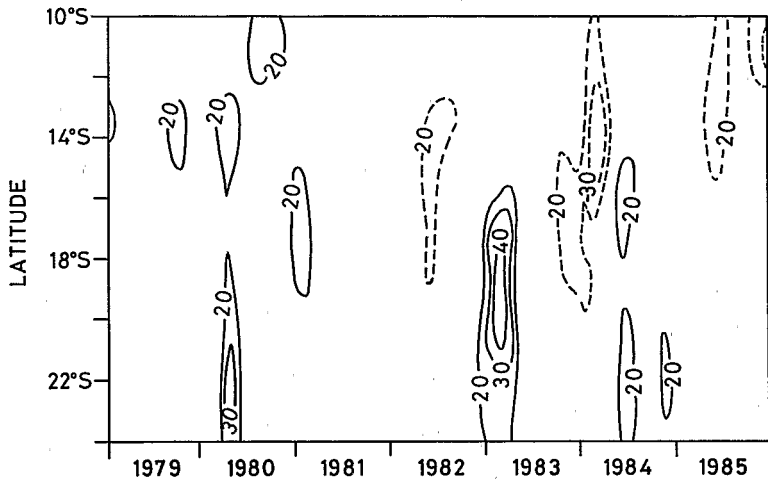


Figure 22. Zonal mean (160E–140W) latent heat flux anomalies ($\text{W} \cdot \text{m}^{-2}$) with reference to the (1979–81 + 1984–85) mean year.

where the saturation vapor temperature is:

$$e_s(T) = 10^{(9.4 - 2352/T)}. \quad (5)$$

Here ρ_a is the air density ($1.2 \text{ kg} \cdot \text{m}^{-3}$), C_e the transfer coefficient or Dalton number as derived from Bunker (1976), L the latent heat of evaporation ($2.5 \cdot 10^6 \text{ J} \cdot \text{Kg}^{-1}$), V the surface wind speed ($\text{m} \cdot \text{s}^{-1}$), T_s the SST (K) and T_a the dry air temperature (K) at the surface both derived from our ORSTOM data base (cf. 2.b), γ the relative humidity (0.8), and P_a the atmospheric pressure at the surface (1013 hPa). Then, the latent heat flux anomalies (re. 1979–81 + 1984–85) have been calculated, and the zonal mean (160E–140W) is presented in Figure 22. The strongest positive pattern ($>20 \text{ W} \cdot \text{m}^{-2}$) occurs south of 15S between December 1982 and April 1983, and mostly reflects the northward wind speed increase as can be deduced from Figure 18. Values over $20 \text{ W} \cdot \text{m}^{-2}$ are in close time agreement with the SST anomalies, and sufficient to cool a 50 m mixed layer by 1°C in five months, as observed in the southern SWTP. Hence, despite the uncertainties of latent heat flux calculations (e.g. Liu, 1988) this corroborates the role of local evaporation in cooling the western tropical Pacific SST during the 1982–83 ENSO (Meyers *et al.*, 1986).

c. Mechanism of sea surface salinity changes. The seasonal SSS cycle appears during the 1979–81 + 1984–85 period with minimum SSS in March/April of each year (Fig. 16). It is due to water advection, vertical mixing and/or *E-P* variations. Of the three factors that influence the seasonal SSS cycle, *E-P* is the only one examined here (the geostrophic salt advection $Ug \cdot S_x$ does not present a seasonal cycle during the referenced period, and vertical mixing effects are not investigated due to the lack of

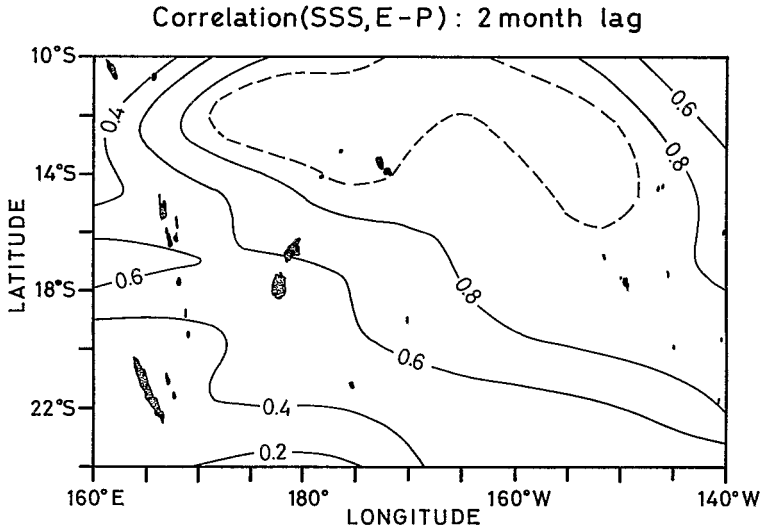


Figure 23. Correlation coefficients between sea surface salinity and evaporation minus precipitation mean years for two month lag. Contour intervals at 0.2 except for the broken line which denotes the 0.9 value.

information on the seasonal variations of the vertical salinity gradient S_z). To this end, mean monthly values of SSS were compared with mean monthly values of $E-P$ where E is $Q_e/(L \cdot \rho_a)$ converted in $\text{m} \cdot \text{month}^{-1}$ (Eq. 3), and P is derived from the maps of Taylor (1973). We must be aware that SSS and E mean years are thus defined over the 1979–81 + 1984–85 period as opposed to P mean year which has been calculated over a much longer and different period. Significant correlations between SSS and $E-P$ ($R > 0.7$) are best obtained for 2–3 month lags between the twelve month series, i.e. minimum SSS 2–3 months after minimum $E-P$. Values $R > 0.7$ are situated along the mean SPCZ position, east of 170E (Fig. 23). They mostly reflect rainfall contribution to $E-P$ since E is in phase with P but one order of magnitude smaller ($E \approx 10\%P$), in agreement with Weare (1982). In other words, minimum SSS occurs two to three months after maximum P . In the $R > 0.7$ region, the annual harmonic of $E-P$ accounts for more than 85% of the total $E-P$ variance so that $E-P$ may be reasonably written as:

$$E - P = (E - P)_0 \cdot \cos(\omega \cdot t - \theta) \quad (6)$$

where ω is the annual frequency and θ is about one month. Minimum $E-P$ thus occurs in January ($\theta = 1$) when wind convergence and precipitation are maximum (e.g. Pazan and Meyers, 1982; Kiladis and Van Loon, 1988). In these conditions, Hires and Montgomery (1972) have shown that if variations of SSS are entirely governed by $E-P$, the minimum SSS would occur 3 months (i.e. a quarter cycle) after the minimum $E-P$. Thus, where $R > 0.7$, the phases between SSS and $E-P$ are properly related and we can conclude that the necessary condition for only $E-P$ governs the SSS changes is satisfied.

The question remains whether the $E-P$ variations are large enough to explain the observed SSS variations. According to Hires and Montgomery (1972), if a uniform mixed layer of density ρ , thickness d and average salinity S_0 is exposed to a variation in $E-P$ of amplitude $(E-P)_0$, the amplitude of the salinity variation is given by:

$$S_1 = (E \cdot P)_0 S_0 / \omega \cdot \rho \cdot d. \quad (7)$$

The thickness d that would be required to assert that annual variations in $E-P$ account for annual variations in SSS were computed over the $R > 0.7$ region. The results show that d should range between extremes of 17 and 44 m, with a mean value of 28 ± 7 m. Whether or not d corresponds to the *in-situ* mixed layer (in density) cannot be verified in the absence of CTD stations in the investigated area. However, inspection of discrete vertical density data (10/25 m sampling) obtained during the DANAIDES (Crémoux, 1980) and HYDROPOL (Wauthy, personal communication) cruises suggests *in-situ* d between 20 and 70 m, i.e. about the same to twice as much as the calculated one. Hence, this last comparison, together with the phase agreement between the SSS and $E-P$ signals, suggests that $E-P$, i.e. mostly P , governs the SSS cycle below the mean SPCZ position.

The low frequency curve in Figure 16 showed the drastic 1982–83 SSS changes mostly located along the mean SPCZ axis where no significant latent heat flux anomalies were observed (Fig. 22). Hence, three processes could have been responsible for the unusual salty water. Firstly, the southern branch of the SEC extended over the SWTP from mid-1982 to mid-1983 (see Section 3c) bringing water of higher salinity. Secondly, salty water arising from the high salinity core of the south tropical Pacific (cf Delcroix *et al.*, 1987-Fig. 3), may be raised to the surface through the aforementioned upwelling process (cf Fig. 21). Thirdly, following typical ENSO developments (Rasmusson and Carpenter, 1982) the SPCZ shifted equatorward, leading to a notable rainfall deficit below its usual position (Ardanuy *et al.*, 1987; Ropelewski and Halpert, 1987) and thus to unusually high SSS. It is likely that advection, vertical mixing and rainfall deficit contribute to increase SSS in the 1982–83 period. The contribution of these three factors was calculated on different grid points, and it is tentatively presented here at 12S–170W. *Salt advection*: our geostrophic calculations (see also Kessler and Taft, 1987) show that the southern branch of the SEC (U_g) accelerated westward by $10 \text{ cm} \cdot \text{s}^{-1}$ between mid-1982 and mid-1983. With one unit of salinity change over 40° longitude (Fig. 15), the advective SSS term $U_g \cdot S_x$ is about 0.35 per year, which is consistent but insufficient to account for the observed SSS increase. *Vertical mixing*: if the fluxes of heat and salt into the surface are $A \cdot T_z$ and $A \cdot S_z$ with A an eddy diffusivity, then the increase in surface salinity δS during the 1982–83 ENSO might be expected to be roughly $\delta T \cdot (A \cdot S_z / A \cdot T_z)$, where δT is the increase of SST due to the 1982–83 ENSO. (i.e., about -0.5°C to -1°C). The disturbed profiles of S_z are not available, but we believe it reasonable to assume that the ratios (S_z/T_z) are probably increased in 1982–83, in the same ratio that the long term mean.

From Levitus' (1982) Figures 12, 13, 22 and 23 this ratio is about $(35.1-36.0)/(29.0-25.8) = -0.3$ in the top 150 m (at 12S-170W), so we would expect an increase of SSS of 0.15 to 0.3 due to mixing. Such SSS increase is still consistent but insufficient to account for the observed SSS increase. *Rainfall deficit*: if we assume a linear decrease of rainfall from $0.2 \text{ m} \cdot \text{month}^{-1}$ in mid-1982 (the mean June value; Taylor, 1973) to 0 in mid-1983 (Ardanuy *et al.*, 1987) this gives a -1.2 m freshwater deficit over a one-year period. Alone, such a deficit would induced a 0.8 SSS rise over a 50 m mixed layer, i.e., the same order of magnitude as observed by mid-1983. Consequently, we suggest that the combined effects of advection, mixing and rainfall reduction upon SSS changes are consistent, i.e. all of the same sign, with the observed SSS increase, and mixing and advection together have the same order of magnitude as the effect of reducing rainfall.

5. Conclusions

In the first part of this paper, we analyzed the main subsurface and surface structures of the Southwestern Tropical Pacific (SWTP), from temperature profiles (8500) and SSS samples (23000) collected during the 1979-85 period. This large amount of data enables us to describe the vertical thermal structure, 0-400 m heat content, geostrophic circulation, SST, and SSS, both for the mean patterns (1979-81 + 1984-85) and for the 1979-85 variability. Special emphasis was put upon the modifications observed during the strong 1982-83 ENSO event. These descriptive aspects usefully complement previous TOGA related studies which, so far, mostly focused north of 10S.

In the second part of the paper, we identified specific mechanisms responsible for the observed SWTP seasonal and ENSO-related variability. The role of these mechanisms is summarized in the three following paragraphs.

a. Vertical thermal structure. In the SWTP, which is a transition zone between the equatorial band and the extra-tropical latitudes, the vertical thermal structure changes present: (i) a marked seasonal cycle in the upper 100 m, in response to variations of the sun position, and (ii) a strong interannual ENSO-related variability, mostly perceivable below 100 m and north of 15S, which results, in 1982-83, from a modification of the local wind stress that strongly raises the thermocline through Ekman pumping.

b. Sea surface temperature. In the northern SWTP (i.e. in the warm pool area), the local Ekman pumping mechanism is also responsible for the negative ENSO-related SST anomalies observed in early 1983. This mechanism uplifts the thermocline and modifies the whole water column all the way to the surface. At this time, similar SST anomalies also appear in the southern SWTP, concomitant with positive latent heat flux anomalies ($>20 \text{ W} \cdot \text{m}^{-2}$) which were sufficient to account for the SST cooling anomalies.

c. Sea surface salinity. Below the mean SPCZ position, phase and amplitude of SSS annual cycle versus precipitation suggests that the rainfall regime associated with the seasonal SPCZ migration is the main process governing the annual SSS cycle (during a "normal" period). During the 1982–83 ENSO event, drastic SSS changes (as much as +1 over the mean SSS) occurred below the mean SPCZ position, evidencing that a rainfall deficit related to the equatorward shift of the SPCZ was the main mechanism responsible for these SSS changes. To a lesser extent, geostrophic advection of saltier water and vertical mixing also contributes to the SSS increase between 10S and 15S.

The above findings suggest that most of the oceanic variability in the SWTP is related to the presence of the SPCZ. In addition, meteorological observations together with numerical model results (Kiladis and Van Loon, 1988; Von Storch *et al.*, 1988) suggest that oceanic behavior in the SWTP affects the position and intensity of the SPCZ. Given the fact that the Tahiti-Darwin SOI, related to the strength of the SPCZ, was used as a primary factor in diagnosing ENSO events, it would not be surprising that air-sea interaction mechanisms over the SWTP are key elements in the development of ENSO event. Quantifying the role of such mechanisms over the whole warm pool area is the challenge of the future COARE program.

Acknowledgments. Once again, we are most thankful to the officers and crews of numerous merchant and navy ships which voluntarily participated in the surface and XBT programs. The contributions of V. Fabre and J. Picaut in collecting and validating additional temperature profiles used in this study have been much appreciated. The wind data were generously made available to us by J. O'Brien of the Florida State University. Comments from ORSTOM colleagues in Nouméa on an earlier version of the manuscript are gratefully acknowledged. Special thanks go to J. Picaut for encouraging us to improve an earlier manuscript. P. Waigana drew the final figures with his usual skill and patience, and M. Laplagne gave pertinent editing suggestions.

REFERENCES

- Ardanuy, P., P. Cuddapah and H. Lee Kyle. 1987. Remote sensing of water vapor convergence, deep convection and precipitation over the tropical Pacific Ocean during the 1982–83 El Niño. *J. Geophys. Res.*, 92, 14204–14216.
- Barnett, T. 1984. Long-term trends in surface temperature over the oceans. *Mon. Wea. Rev.*, 112, 303–312.
- Bunker, A. 1976. Computations of surface energy flux and annual air-sea interaction cycles of the North Atlantic Ocean. *Mon. Wea. Rev.*, 104, 1122–1140.
- Crémoux, J. L. 1980. Résultats des croisières tropicales du centre ORSTOM de Nouméa (1967–1977); II partie: Pacifique central. *Rapports scientifiques et techniques*, 15. Centre ORSTOM de Nouméa, Nouvelle Calédonie (New Caledonia).
- Delcroix, T., G. Eldin and C. Hénin. 1987. Upper ocean water masses and transports in the western tropical Pacific (165E). *J. Phys. Oceanogr.*, 17, 2248–2262.
- Delcroix, T. and C. Gautier. 1987. Estimates of heat content variations from sea level measurements in the central and western tropical Pacific from 1979 to 1985. *J. Phys. Oceanogr.*, 17, 725–734.

- Delcroix, T. and C. Hénin. 1989. Atlas océanographique du pacifique tropical sud-ouest. Centre ORSTOM de Nouméa, Nouvelle Calédonie (New Caledonia). Série science de la mer, océanographie physique, 68 pp.
- Donguy, J. R. and A. Dessier. 1983. El Niño-like events observed in the tropical Pacific. *Mon. Wea. Rev.*, *111*, 2136–2139.
- Donguy, J. R., G. Eldin, A. Morlière and J. P. Rébert. 1984. Variability of dynamic topography and equatorial currents in relation to hydroclimatic conditions in the western Pacific. *Océanographie tropicale*, *19*, 155–161.
- Donguy, J. R. and C. Hénin. 1975. Evidence of the south tropical counter-current in the Coral Sea. *Aust. J. Mar. Freshwat. Res.*, *26*, 405–409.
- 1976. Relations entre les précipitations et la salinité de surface dans l'océan Pacifique tropical sud-ouest basées sur un échantillonnage de surface de 1956 à 1973. *Annales Hydrogr.*, série No 5, *4*, 53–59.
- 1978. La salinité de surface dans l'océan Pacifique tropical sud ouest. *Cahiers ORSTOM*, série Océanogr., *16*–2, 107–136.
- Donguy, J. R., C. Hénin, F. Jarrige and F. Rougerie. 1974. Esquisse dynamique et hydrologique du pacifique central sud. *Cahiers ORSTOM*, série Océanogr., *12*–2, 129–139.
- Folland, C., D. Parker and F. Kates. 1984. Worldwide marine temperature fluctuations 1856–1981. *Nature*, *310*, 670–673.
- Goldenberg, S. and J. O'Brien. 1981. Time and space variability of tropical Pacific wind stress. *Mon. Wea. Rev.*, *109*, 1190–1207.
- Harrison, D. E. 1984. On the appearance of sustained westerlies during the 1982 Pacific warm event. *Science*, *224*, 1099–1102.
- He, Y. and W. White. 1987. Interannual variability of the Kuroshio frontal structure along its western boundary in the North Pacific Ocean associated with the 1982 ENSO event. *J. Phys. Oceanogr.*, *17*, 1494–1506.
- Heddinghaus, R. and A. Krueger. 1981. Annual and interannual variations in outgoing longwave radiation over the tropics. *Mon. Wea. Rev.*, *109*, 1208–1212.
- Hires, R. and R. Montgomery. 1972. Navifacial temperature and salinity along the track from Samoa to Hawaii, 1957–1965. *J. Mar. Res.*, *30*, 177–200.
- Kessler, W. and B. Taft. 1987. Dynamic heights and zonal geostrophic transports in the central tropical Pacific during 1979–84. *J. Phys. Oceanogr.*, *17*, 97–122.
- Kiladis, G. and H. Van Loon. 1988. The southern oscillation. part VII: Meteorological anomalies over the Indian and Pacific sectors associated with the extremes of the oscillation. *Mon. Wea. Rev.*, *116*, 120–136.
- Large, W. and S. Pond. 1981. Open ocean momentum flux measurements in moderate to strong wind. *J. Phys. Oceanogr.*, *11*, 324–336.
- Leetmaa, A. and J. Witte. 1984. El Niño Atlas 1982–83. Leetmaa and Witte, eds., NOAA/ADML, Miami, Florida, 159 pages.
- Lemasson, L. and B. Piton. 1968. Anomalie dynamique de la surface de la mer le long de l'équateur dans l'océan Pacifique. *Cahiers ORSTOM*, série Océanogr., *6*, 39–45.
- Levitus, S. 1982. Climatological Atlas of the World Ocean. US Dept. of Commerce, NOAA, 173 pp.
- Liu, T. 1988. Moisture and latent heat flux variability in the tropical Pacific derived from satellite data. *J. Geophys. Res.*, *93*, 6749–6760.
- Lorenz, E. 1956. Empirical orthogonal functions and statistical weather prediction. Rep. No. 1, Statistical Forecasting Program, MIT, 49 pp.
- Lukas, R. 1987. On the role of western Pacific air-sea interaction in the El-Niño/Southern Oscillation phenomenon. Proceedings of the U.S. TOGA western Pacific air-sea interaction workshop. USTOGA-8, 207 pages. Compiled and edited by R. Lukas and P. Webster.

- Lukas, R. and P. Webster. 1987. TOGA-COARE: a coupled ocean-atmosphere response experiment for the warm pool regions of the western Pacific. Compiled by R. Lukas and P. Webster.
- McPhaden, M., A. Busalacchi and J. Picaut. 1988. Observations and wind-forced model simulations of the mean seasonal cycle in tropical Pacific sea surface topography. *J. Geophys. Res.* 93, 8131–8146.
- Merle, J., H. Rotschi and B. Voituriez. 1969. Zonal circulation in the tropical western South Pacific at 170E. *Bulletin of the Japanese Society of Fisheries Oceanography, Special Number (Prof. Uda's commemorative papers)*, 91–98.
- Meyers, G. 1982. Interannual variation in sea level near Truk Island. A bimodal seasonal cycle. *J. Phys. Oceanogr.*, 12, 1161–1168.
- Meyers, G. and J. R. Donguy. 1984. South equatorial current during the 1982–83 El Niño. *Tropical Ocean Atmosphere Newsletter*, 27, 10–11.
- Meyers, G., J. R. Donguy and R. K. Reed. 1986. Evaporative cooling of the western equatorial Pacific Ocean by anomalous winds. *Nature*, 323, 523–526.
- Mitchum, G. 1987. Trade wind fluctuations associated with El Niño/Southern oscillation events. *J. Geophys. Res.*, 92, 9464–9468.
- North, G., T. Bell, R. Cahalan and F.J. Moeng. 1982. Sampling errors in the estimation of the empirical orthogonal functions. *Mon. Wea. Rev.*, 110, 699–706.
- Oudot, C. and B. Wauthy. 1976. Upwelling et dôme dans le Pacifique tropical occidental: distributions physico-chimiques et biomasse végétale. *Cahiers ORSTOM, série océanogr.*, 14-1, 27–49.
- Pazan, S. and G. Meyers. 1982. Interannual fluctuations of the tropical Pacific wind field and the southern oscillation. *Mon. Wea. Rev.*, 110, 587–600.
- Pazan, S. and W. White. 1987. Short term climatic variability in the volume budget of the western tropical North Pacific during 1979–82. *J. Phys. Oceanogr.*, 17, 440–454.
- Quinn, W., V. Neal and S. Antunez de Mayolo. 1987. El Niño occurrences over the past four and a half centuries. *J. Geophys. Res.*, 92, 14449–14461.
- Rasmusson, E. and T. Carpenter. 1982. Variations in tropical sea surface temperature and surface wind fields associated with the southern oscillation/El Niño. *Mon. Wea. Rev.*, 110, 354–384.
- Reid, J. and R. Arthur. 1975. Interpretation of maps of geopotential anomaly for the deep Pacific Ocean. *J. Mar. Res.*, 33(Suppl.), 37–52.
- Reverdin, G. 1988. Sea surface temperature: a comparison between ship reports from marine decks and ship-of-opportunity subsurface data in the tropical Atlantic ocean. *Tropical Ocean Atmosphere Newsletter*, 47, 1–4.
- Ropelewski, C. and M. Halpert. 1987. Global and regional scale precipitation patterns associated with the El Niño/Southern oscillation. *Mon. Wea. Rev.*, 115, 1606–1626.
- Rotschi H., P. Hisard and F. Jarrige. 1972. Les eaux du Pacifique occidental à 170E entre 20S et 4N. *Travaux et documents de l'ORSTOM*, 19. Centre ORSTOM de Nouméa, Nouvelle Calédonie (New Caledonia).
- Sadler, J. and B. Kilonsky. 1985. Deriving surface winds from satellite observations of low level cloud motions. *J. Climate Appl. Meteor.*, 24, 758–769.
- Stevenson J. and P. Niiler. 1983. Upper ocean heat budget during the Hawaii to Tahiti shuttle experiment. *J. Phys. Oceanogr.*, 13, 1894–1907.
- Taylor, R. 1973. An atlas of Pacific islands rainfall. Hawaii Institute of Geophysics, University of Hawaii, Rep. HIG-73-9. Available from National Technical Information Service, Springfield, VA 22151, USA.
- Van Loon, H. and D. Shea. 1985. The southern oscillation. Part IV: the precursors south of 15S to the extremes of the oscillation. *Mon. Wea. Rev.*, 113, 2063–2074.

- 1987. The Southern oscillation. Part VI: anomalies of sea level pressure on the southern hemisphere and of Pacific sea surface temperature during the development of a warm event. *Mon. Wea. Rev.*, *115*, 370–379.
- Von Storch, H., H. Van Loon and G. Kiladis. 1988. The southern oscillation. Part VIII: Model sensitivity to SST anomalies in the tropical and subtropical regions of the South Pacific convergence zone. *J. Climate*, *1*, 325–331.
- Walker, G., 1923. Correlation in seasonal variations of weather. VIII: a preliminary study of world weather (World weather I). *Memoirs India Meteorol. Dept.*, *24*, 75–131.
- WCRP. 1985. World Climate Research Program publications series No 3, Scientific plan for the Tropical Ocean and Global Atmosphere Program. World meteorological organization, 146 pp.
- Weare, B. 1982. El Niño and the tropical Pacific Ocean surface temperature. *J. Phys. Oceanogr.*, *12*, 17–27.
- Weare, B., P. Strub and M. Samuel. 1981. Annual mean surface heat fluxes in the tropical Pacific Ocean. *J. Phys. Oceanogr.*, *12*, 705–717.
- White, W. B., G. Meyers, J. R. Donguy and S. Pazan. 1985. Short term climatic variability in the thermal structure of the Pacific Ocean during 1979–1982. *J. Phys. Oceanogr.*, *15*, 917–935.
- Wyrski, K. 1975. Fluctuations of the dynamic topography in the Pacific Ocean. *J. Phys. Oceanogr.*, *5*, 450–459.
- 1984. A southward displacement of the subtropical gyre in the south Pacific during the 1982–83 El Niño. *Tropical Ocean Atmosphere Newsletter*, *23*, 14–15.
- Wyrski, K. and B. Kilonsky. 1984. Mean water and current structure during the Hawaii to Tahiti shuttle experiment. *J. Phys. Oceanogr.*, *14*, 242–254.
- Wyrski, K. and G. Meyers. 1976. The trade wind field over the Pacific Ocean. *J. Applied Met.*, *15*, 698–704.
- Yoshida, K. and L. Mao. 1957. A theory of upwelling of large horizontal extent. *J. Mar. Res.*, *16*, 40–57.